Universidade de Aveiro
Ano 2021

Maria Simone Fernandes Soares

Imunossensores de Fibra Ótica Baseados em SPR para a Deteção de Cortisol

Optical Fiber Immunosensors Based on SPR for Cortisol Detection

Universidade de Aveiro
Ano 2021

Maria Simone Fernandes Soares

Imunossensores de Fibra Ótica Baseados em SPR para a Deteção de Cortisol

Optical Fiber Immunosensors Based on SPR for Cortisol Detection

Dissertação apresentada à Universidade de Aveiro para cumprimento dos requisitos necessários à obtenção do grau de Mestre em Engenharia Biomédica, realizada sob a orientação científica do Doutor Carlos Alberto Ferreira Marques, Investigador Auxiliar do Departamento de Física da Universidade de Aveiro, e do Doutor Nuno Miguel Franco dos Santos, Investigador de Pós-doutoramento do Departamento de Física da Universidade de Aveiro.

Dedico este trabalho aos meus pais e às minhas irmãs pela oportunidade proporcionada e pelo constante apoio.

o júri / the jury

presidente / president

Professora Doutora Ana Luísa Monteiro Silva
Professora Auxiliar do Departamento de Física da Universidade de Aveiro

vogais / examiners committe

Professor Doutor Paulo Sérgio De Brito André
Professor Catedrático do Departamento de Eletrónica da Universidade de Lisboa

Doutor Carlos Alberto Ferreira Marques
Investigador Auxiliar do Departamento de Física da Universidade de Aveiro

agradecimentos/ acknowledgments

Em primeiro lugar, gostaria de agradecer ao Doutor Carlos Alberto Ferreira Marques pelo conhecimento transmitido e pela constante disponibilidade e prontidão no acompanhamento e orientação neste trabalho. Gostaria também de agradecer ao Doutor Nuno Miguel Franco dos Santos pelo auxílio e coorientação ao longo deste trabalho.

Queria agradecer da mesma forma à Doutora Sónia Oliveira Pereira e à Doutora Cátia Sofia Jorge Leitão pelo incansável apoio, disponibilidade, ajuda e orientação durante a realização deste trabalho.

Gostaria também de agradecer ao meu amigo Miguel Vidal pelas partilhas de conhecimento e pela ajuda incansável ao longo da realização deste trabalho.

Queria também de deixar umas palavras de agradecimento à Professora Doutora Margarida Maria Resende Vieira Facão pelo conhecimento transmitido, pela disponibilidade e ajuda incansáveis na simulação das fibras óticas.

Agradeço à Doutora Ana Catarina Fernandes Moreirinha pela aquisição de dados de ATR-FTIR.

Agradeço também ao Professor Doutor Christophe Caucheteur pelo fornecimento das fibras óticas de sílica em *D-shape* e ao Professor Doutor Nunzio Cennamo pelas fibras óticas poliméricas em *D-shape* revestidas com ouro.

Um agradecimento especial aos meus Pais, Irmãs, Avós e demais familiares pelos conselhos e apoio que sempre me proporcionaram.

Por fim, um agradecimento a todos os meus amigos pelo apoio e por todas as experiências vividas.

palavras-chave

Biossensor, cortisol, *D-shape*, fibra ótica polimérica (POF), fibra ótica de sílica (SOF), ressonância de plasmão de superfície (SPR)

resumo

O *stress* é uma resposta fisiológica e comportamental normal a um estímulo que, de alguma forma, perturba a manutenção da homeostase, levando à alteração dos níveis de cortisol (hormona do *stress*). Quando o *stress* é perseverante e descontrolado pode afetar gravemente várias áreas, como a saúde humana e algumas aplicações na biologia marinha, incluindo a produção de aquacultura. Atualmente, a deteção de cortisol é realizada em laboratórios por técnicas convencionais que apresentam várias desvantagens, sendo uma delas o elevado tempo de espera pela resposta. Deste modo, é imprescindível o desenvolvimento de biossensores que detetem o cortisol diretamente no local de interesse (POC, do inglês *point of care*). Os biossensores são dispositivos analíticos miniaturizados capazes de detetar e quantificar biomarcadores específicos. Ademais, permitem a monitorização em tempo real superando as desvantagens das técnicas convencionais.

Fibras ótica de sílica (SOF, do inglês *silica optical fibers*) e fibras ótica poliméricas (POF, do inglês *polymeric optical fibers*) revestidas com ouro (Au) foram utilizadas neste trabalho para desenvolver imunossensores para a deteção de cortisol. Ao longo de todo o processo experimental, foi também efetuada a simulação da resposta ao índice de refração (RI, do inglês *refractive index*) das fibras óticas revestidas com Au de forma a poder comparar os resultados experimentais com os obtidos a partir da simulação. Em laboratório, as fibras revestidas com Au foram inicialmente caracterizadas ao RI com oito concentrações de glicose com RI de 1,333 a 1,386 unidades de RI (RIU, do inglês *refractive index unit*). A sensibilidade obtida com a Au-SOF foi 1646,67 ± 91,66 nm/RIU, sendo inferior à simulada (2138,95 ± 142,65 nm/RIU), e para a Au-POF a sensibilidade apresentou um valor de 1566,81 ± 96,87 nm/RIU, não sendo possível obter resultados pela simulação. Posteriormente, as fibras foram funcionalizadas com o anticorpo (AB, do inglês *antibody*) anti-cortisol e passivadas com albumina do soro bovino (BSA, do inglês *bovine serum albumin*), utilizando a cisteamina que apresenta um grupo tiol e um grupo amina para permitir a ligação ao Au e ao AB, respetivamente. Após este procedimento, ambos os imunossensores foram testados para uma gama de concentrações de cortisol de 0,01 a 100 ng/mL, no qual os imunossensores de SOF apresentaram um desvio total médio do comprimento de onda de ressonância de 3,70 ± 0,39 nm e um limite de deteção (LOD, do inglês *limit of detection*) de 1,46 ng/mL, enquanto que para os imunossensores de POF não foi possível traçar uma reta de calibração. Testes de controlo em sensores funcionalizados com AB anti-cortisol foram também realizados utilizando glicose (50 mg/dL e 500 mg/dL) e colesterol (170 mg/dL e 240 mg/dL). A funcionalização e o teste de deteção dos imunossensores foram acompanhados de caraterização morfológica e química. No final, um teste preliminar de regeneração de um imunossensor de SOF mostrou resultados promissores. Futuramente, será necessário realizar ensaios de regeneração e reutilização para validação do procedimento aplicado.

keywords

Biosensor, cortisol, D-shape, polymeric optical fiber (POF), silica optical fiber (SOF), surface plasmon resonance (SPR)

abstract

Stress is a normal physiological and behavioral response to a stimulus that somehow disturbs the maintenance of homeostasis, leading to changes in cortisol (stress hormone) levels. When stress is persistent and uncontrolled, it can severely affect several areas, such as human health and some applications in marine biology, including aquaculture production. Currently, the detection of cortisol is performed in laboratories using conventional techniques which have several disadvantages, one of them being the long waiting time for a response. Therefore, it is essential to develop biosensors that detect cortisol directly in point of care (POC). Biosensors are miniaturized analytical devices capable of detecting and quantifying specific biomarkers. In addition, they allow real-time monitoring, overcoming the disadvantages of conventional techniques.

Silica optical fibers (SOF) and polymeric optical fibers (POF) coated with gold (Au) were used in this work to develop immunosensors for cortisol detection. Throughout the entire experimental process, simulation of the response to the refractive index (RI) of the optical fibers coated with Au was also carried out to compare the experimental results with those obtained from the simulation. In the laboratory, Au-coated fibers were initially characterized at RI with eight glucose concentrations ranging from 1.333 to 1.386 RI units (RIU). The obtained sensitivity with Au-SOF was 1646.67 ± 91.66 nm/RIU, being lower than the simulated (2138.95 ± 142.65 nm/RIU), and for Au-POF the sensitivity presented a value of 1566.81 ± 96.87 nm/RIU, was not possible to obtain results by the simulation. Subsequently, the fibers were functionalized with anti-cortisol antibody (AB) and passivated with bovine serum albumin (BSA), using cysteamine which has a thiol group and an amine group to allow binding to Au and AB, respectively. After this procedure, both immunosensors were tested for a range of cortisol concentrations from 0.01 to 100 ng/ml, in which the SOF immunosensors had a mean total resonance wavelength shift of 3.70 ± 0.39 nm, and a limit of detection (LOD) of 1.46 ng/mL, whereas for POF immunosensors it was not possible to trace a calibration line. Control tests on sensors functionalized with anti-cortisol AB were also performed using glucose (50 mg/dL and 500 mg/dL) and cholesterol (170 mg/dL and 240 mg/dL). The functionalization and detection test of immunosensors were accompanied by morphological and chemical characterization. Finally, a preliminary test of a SOF immunosensor regeneration showed promising results. In the future, it will be necessary to perform regeneration and reuse tests to validate the applied procedure

Contents

List of Acronyms

AB	Antibody
ADH	Antidiuretic Hormone
AP	Phosphatase
ATR-FTIR	Attenuated Total Reflection-Fourier Transform Infrared
BSA	Bovine Serum Albumin
CFBG	Chirped Fiber Bragg Grating
CRH	Corticotrophin-Releasing Hormone
DI	Deionized water
EDC	*N*-(3- dimethylaminopropyl)-*N'*-ethylcarbodiimide hydrochlorine
EDX	Energy dispersive X-ray analysis
ELISA	Enzyme-Linked Immunosorbent Assay
EW	Evanescent Wave
FBG	Fiber Bragg Grating
GO	Graphene Oxide
HPA	Hypothalamic-Pituitary-Adrenocortical
LC-MS/MS	Liquid Chromatography-Tandem Mass Spectrometry
LOD	Limit of Detection
LPG	Long Period Grating
LS	Logarithmic Sensitivity
LSPR	Localized Surface Plasmon Resonance
MFD	Mode-Field Diameter
MMF	Multimode Fiber
NHS	*N*-hydroxysuccinimide
PBS	Phosphate Buffered Saline
PHFIP 2-FA	Polyhexafluoro isopropyl 2-fluoroacrylate
PMMA	Poly(methylmethacrylate)
POC	Point of Care
POF	Polymeric Optical Fiber
PTFE	Polytetrafluoroethylene
RAS	Recirculating Aquaculture Systems
rGO	Reduced Graphene Oxide
RI	Refractive Index
RIU	Refractive Index Units
SEM	Scanning Electron Microscopy
SMF	Single-Mode Fiber
SOF	Silica Optical Fiber
SPs	Plasmões de Superfície
SPP	Surface Plasmon Polariton
SPR	Surface Plasmon Resonance
TFBG	Tilted Fiber Bragg Grating
TIR	Total Internal Reflection
UV	Ultraviolet

List of Symbols

A_{eff}	Effective area
A_j	Sellmeier coefficients
$\tilde{E}$	Electric field in cylindrical coordinates
E_t	Electric field
GA_j	Sellmeier coefficients for Ge-doped silica
Gl_j	Sellmeier coefficients for Ge-doped silica
$\tilde{H}$	Magnetic field in cylindrical coordinates
I	Intensity
k	Wavenumber
k_0	Wavenumber in vacuum
l_j	Sellmeier coefficients
n	Refractive index of materials
n_{eff}	Effective refractive index
n_{eff}^{core}	Effective index of the core mode
$n_{eff}^{clad\ (m)}$	Effective index of the m^{th} cladding mode
$n_{eff,I}$	Imaginary part of effective refractive index
$n_{eff,R}$	Real part of effective refractive index
n_I	Imaginary part of refractive index
n_R	Real part of refractive index
P	Power
P_{final}	Final power
$P_{initial}$	Initial power
S_n	Sensor sensitivity to the refractive index
T	Transmission
X	Fraction of germanium
α	Attenuation constant
β	Propagation constant
β_I	Imaginary part of propagation constant
β_R	Real part of propagation constant
Δn	Variation of the refractive index
$\Delta\lambda_{res}$	Variation of the resonance wavelength
θ	Tilt angle
Λ	Grating Period
λ	Wavelength
λ_B	Bragg wavelength
λ_0	Wavelength in vacuum
$\lambda_{res\ (m)}^{LPG}$	Resonance Wavelength of at the m^{th} cladding mode of LPG
$\lambda_{res\ (m)}^{TFBG}$	Resonance Wavelength of at the m^{th} cladding mode of TFBG
ω	Frequency

List of Figures

I - Introduction

1.1 Framework and Motivation

Nowadays, daily lifestyle issues are the main cause of psychological stress, which contributes to the health disparities experienced by individuals. Several factors, such as globalization, changed lifestyles, competition, technological progress that leads to increasingly stressful jobs, among others, contribute heavily to the increase in the level of psychological stress. This problem is becoming a serious concern that can affect individuals' daily lives and their health. These challenges are being faced by the most developed countries, which leads to the increasing need for stress monitoring.

Cortisol is popularly designated as the stress hormone since the most dominant effect of cortisol levels variation results from psychological or emotional stress. Although cortisol is considered the stress hormone, is also involved in the regulation of several physiological processes, including blood pressure, glucose levels, and carbohydrate metabolism. Furthermore, it is also important in the homeostasis of the cardiovascular, immune, renal, musculoskeletal, and endocrine systems. Cortisol levels vary through a circadian rhythm over a 24-hour cycle, with higher levels occurring during dawn and lower levels during night-time sleep [1]. When cortisol levels are in excess, they can lead to the development of, for instance, Cushing’s syndrome, while too low cortisol levels can lead to Addison's disease. The first disease is manifested by obesity, fatigue, and bone weakness, and the second presents the following symptoms: weight loss, fatigue, skin blemishes, and difficulty in healing [2].

Currently, chronic stress is known to trigger disorders like depression and cardiovascular diseases. Therefore, tools capable of monitoring stress have been developed with great effort, in which cortisol is the target biomarker. Analysis of cortisol levels in the human body can be performed using blood, hair, urine, interstitial fluids, saliva, or sweat samples. However, a sample that contains several biomarkers, health indicators, and is a great alternative to blood (which the latter has an invasive sampling), is sweat. Besides, it can be obtained from several locations of the body surface in a non-invasive way [1], [3].

On the other hand, aquaculture is one area where stress has also a high impact. Aquaculture production has been widely performed in recirculating aquaculture systems (RAS) in the last years. When small variations in water chemistry/quality occur, stress can be induced, reducing food intakes, which not only leads to a reduced fish growth performance but also can lead to mortality when acute or chronic stress is high. In this way, it is essential to monitor cortisol in water fish tanks daily, which is not happening at all [4], [5].

In both cases, cortisol can be detected by various conventional laboratory techniques, which use equipment that must be operated by specialized people and require sample transportation to laboratories, increasing the time from sampling to the result. To overcome these drawbacks, miniaturized devices capable of detecting and quantifying specific analytes as biosensors are essential. The use of these devices has advantages in point of care (POC) compared to traditional techniques.

A biosensor is an analytical device that comprises three distinct components: a biorecognition element, which binds (recognizes) the analyte or analytes of interest; a transducer which converts the signal resulting from the analyte and biorecognition element interactions into a signal that can

be measured and quantified; and a reading system that contains electronic processors and associated signals, which are primarily responsible for presenting the results [6]. Lately, high-affinity anti-cortisol ABs have been used as the recognition element for the development of biosensors for cortisol detection [7], [8], in which immunosensors for cortisol detection have several advantages, such as increased sensitivity, decreased limit of detection (LOD), ease of use, cost-effectiveness, and the need for expensive reagents is reduced [9].

Surface plasmon resonance (SPR) is a phenomenon that has attracted enormous attention over the last three decades. This phenomenon allows a rapid and accurate optical detection of various parameters, such as physical, chemical, and biochemical [10]. When free electrons collectively oscillate in metal, surface plasmons (SPs) are created. SPs propagate along a dielectric-metal interface and can be excited by the evanescent wave (EW) (which decays exponentially) generated from incident light. When the propagation constants (wave vector and frequency) of the EW are similar to those of the SPs, the SPR phenomenon is triggered. The resonance condition is very sensitive to changes in the refractive index (RI) of the surrounding medium. As a result, these changes can be determined by analyzing the resonance condition [10].

The most used configuration for SPR is the Kretschmann configuration, in which a prism with a high RI is coated with a metallic layer, which allows SPs excitation by the EW of the prism. The EW is created from the total internal reflection (TIR) the occurs inside the prism. However, these planar SPR sensors are bulky in size and cannot be applied in remote sensing. As a result, optical fiber SPR sensing emerged, offering simplified and flexible optical design, remote sensing, miniaturized and *in situ* measurements [10]. Due to the several advantages, optical fiber detection based on SPR has been the subject of study in a large number of investigations in different areas [11]. Nowadays, several optical fiber configurations, like uncladded, D-shaped, U-shaped, tapered, end-face reflected, grating-modified, and different plasmonic materials have been studied to improve the performance and sensitivity of the optical fiber SPR sensors.

As plasmonic materials, most commercially available SPR sensors and those presented in the literature employ gold (Au) and/or silver (Ag). Nonetheless, Au has some advantages over Ag, such as chemical stability and better SPR performance, whereas Ag tends to oxidize when exposed to air, which impairs its performance and contributes to a short lifespan. A material that has recently been shown to be promising in this area is graphene. When graphene is deposited on the metal film, the electric field increases, and, therefore, the performance of the sensors is considerably improved. Due to π-π interactions, graphene also allows better adsorption of biomolecules, leading to a high affinity of the system for those biorecognition molecules [12]. Besides graphene, other materials have also been studied for this purpose, such as graphene oxide (GO), reduced graphene oxide (rGO), zinc oxide (ZnO), among others.

To conclude, several factors fundamentally present in developed countries, mainly technological advances, have contributed to the presence or significant increase of stress. As a result, the monitoring of the so-called stress hormone (cortisol) has been increasingly the motive of research in different areas, with the purpose of minimizing damage caused by stress and increase the quality of life in an increasingly digital and industrialized world.

1.2 Thesis Objectives

The present dissertation focuses on the development and characterization of optical fiber immunosensors for cortisol detection with the purpose of using them, in the future, in biomedical and biological applications, for instance, biosensors that detect cortisol in human sweat (via smart bandage) and water fish tanks.

In this sense, the dissertation begins with the presentation of bibliographical and scientific research on the subject, aiming to acquire knowledge and theoretical foundations, following by the methodology that was applied.

In order to create these biosensors, the dissertation focus on the study of two types of optical fibers, silica optical fibers (SOF) and polymeric optical fibers (POF) with D-shape configuration, to allow the interaction of the EW with the surrounding medium. Au is deposited on the surface of the fibers (by sputtering method) to trigger the SPR phenomenon.

Before the experimental procedures, a section is presented with the simulation of the referred structures in order to compare some experimental results with the simulated ones. Experimentally, the next step consists of the optical characterization of the immunosensors to ascertain their sensitivity RI.

Afterward, Au functionalization with anti-cortisol ABs is carried out to allow, at the time of detection, the formation of AB-antigen immunocomplex, and then, the functionalized immunosensors are tested for different cortisol concentrations. Biosensor response is studied by analyzing the SPR signature in the transmission spectra. After this process, control tests are performed with glucose and cholesterol as interferents to ascertain the specificity of immunosensors.

Finally, Au-SOF immunosensors are characterized and analyzed by scanning electron microscopy (SEM) and attenuated total reflection-Fourier transform infrared (ATR-FTIR) techniques to evaluate the surface morphology and chemical composition, and the presence of proteins resulting from functionalization, respectively.

In addition, a short section with preliminary results for SOF reuse is presented, in which a chemical method of removing the thiol groups (resulting from functionalization) from the Au surface is used using a mixture of ammonium hydroxide (NH_4OH), hydrogen peroxide (H_2O_2), and DI water (H_2O). In this case, the immunosensors are analyzed by ATR-FTIR.

Although two studies with SOF and POF have already been carried out at the University of Aveiro, this work presents differences concerning those studies in order to improve the cortisol detection process in several aspects. In one of those studies, a TFBG was used instead of a D-shape SOF to fabricate a biosensor, in which the manufacturing process is more expensive, and it is not always easy to obtain very similar TFBG spectra, affecting the reproducibility. In the other study, a POF with an unclad structure coated with gold-palladium (AuPd) alloy was used. In the present work, instead of AuPd alloy, is used Au coated on a D-shape POF and SOF to produce plasmonic biosensors for cortisol detection and quantification.

II - State of the Art

2.1 Stress Hormone: Cortisol

The profound physiological consequences of stress were empirically demonstrated for the first time by Hans Selye in 1936 in his article, “A Syndrome Produced by Diverse Nocuous Agents” [13]. Selye, after almost 40 years of overly productive research, declared: “Everybody knows what stress is and nobody knows what it is” [14], which shows the dilemma in finding a definition for stress syndrome [14]. Nonetheless, pragmatic approaches define stress as a normal physiological and behavioral response to something that has happened or is about to happen and, in some way, disturbs the homeostasis. Therefore, changes caused by stress range from behavioral to molecular adaptations, in which, the molecules that transmit these messages are designated stress hormones [15].

When hormonal changes caused by stress do not normalize, some clinical conditions with great socio-economic importance, such as age-related cognitive decline, neurodegenerative diseases, cardiovascular disorders, diabetes, and abdominal obesity, are aggravated. In addition, persistent and uncontrollable stress is pathological and can induce diseases like depression, which is the most prominent example [15].

Stress implies a large number of neuronal circuits, such as the prefrontal cortex, hippocampus, amygdala, septum, and hypothalamus, which results in the activation of the hypothalamic-pituitary-adrenocortical (HPA) axis. As a result, the production of corticotrophin-releasing hormone (CRH) and antidiuretic hormone (ADH) in the paraventricular nuclei of the hypothalamus is stimulated. Subsequently, both neuropeptides reach the pituitary gland through small blood vessels (in the case of CRH) or neural projections (in the case of ADH), which results in the secretion and release of CRH into the bloodstream, leading to the stimulation of the cortex of the adrenal gland to synthesize and release glucocorticoids, in particular cortisol [15].

Hereupon, cortisol plays an important role in human homeostasis maintenance. Although some changes in human homeostasis are beneficial to the body, protracted exposure to these stimuli results in an abnormal increase in cortisol secretion that has a high effect on the immune, skeletal, cardiovascular, endocrine, and renal systems, as well as on the metabolic levels of glucose, blood pressure, and carbohydrates [3]. During the day, blood cortisol levels change, which the higher level happens in the early morning (30 minutes after waking, 5-25 µg/dL or 50-250 ng/mL) and the lowest before bedtime (3-13 µg/dL or 30-130 ng/mL) [16], [17], as can be seen from the example in **Figure 1**. In sweat, a study showed that cortisol levels range from 8.16 ng/mL to 141.70 ng/mL, with the highest levels occurring in the morning and the lowest in the evening, as in blood [18]. The abnormal wane of cortisol can lead to Addison disease and high levels of Cushing syndrome. Consequently, can lead to severe fatigue, anxiety, obesity, cognitive difficulties, depression, and cardiovascular diseases [16]. Exposure to psychological, environmental, or emotional stress can lead to a substantial variation in cortisol levels [3]. In this way, cortisol is considered the main stress biomarker.

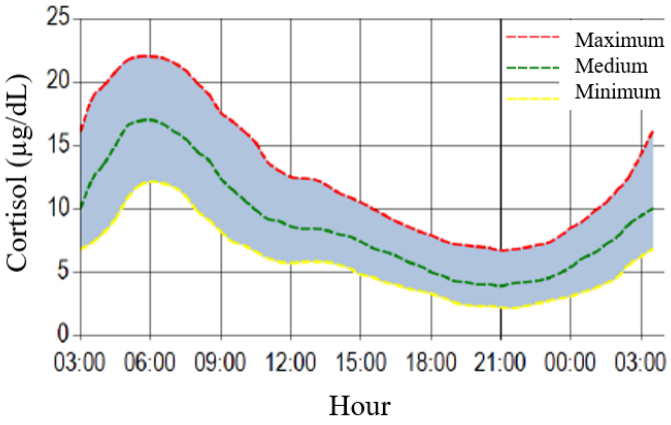

Figure 1 - Plasma cortisol levels. Adapted from [19].

Conventional laboratory detection techniques for cortisol quantification consist of separation methods, like chromatography, or immunoassays. Chromatographic techniques are the oldest and one of the first to be developed for cortisol detection [2]. These techniques were first described by Kabra et al. in 1979 [20], and are used to separate cortisol from the various biofluids, using a mass transfer-induced adsorption process. In turn, immunoassays are related to the ability of an AB to recognize and selectively bind to an antigen, known as an analyte. Immunoassays are the standard technique for detecting the presence and measuring the concentration of the analyte of interest due to the high degree of selectivity and specificity of an AB-antigen bond [2]. Among the several immunoassays for cortisol detection, the first to be reported was the radioimmunoassay in the early 70s [21], [22] and, then, the fluorimetric assay [23], [24] since in radioimmunoassays were used radioisotopes that could cause potential nocive effects. Furthermore, the flow immunoassay and the enzyme-linked immunosorbent assay (ELISA) were also reported for cortisol detection. ELISA is the standard immunoassay for determining protein concentration because is the most sensitive and versatile technique [2]. With the purpose to detect cortisol, this immunoassay was performed for the first time in 1985 by Lewis and Elder [25] and, after, by Shimada *et al*. in 1995 [26].

Although these methods offer high sensitivity, they have many disadvantages, such as they are time-consuming, involve reactions with various steps, require a laboratory for clinical analysis, and experienced professionals, among others [1]. To overcome these drawbacks, it is crucial to develop diagnostic tools capable of quantifying specific biomarkers and provide useful information in health to use in POC.

Further, cortisol is also considered an important stress biomarker in some marine biology applications. One example is in the field of aquaculture, where this hormone proved to be a reliable stress indicator in fishes. The assessment of the stress levels of fishes in aquaculture, directly in the water, is extremely important to understand his interaction with growth, reproduction, the immune system, and the adequacy of fishes to the environment and water quality [27]. In the last decade, the production of aquaculture in intensive systems has increased rapidly, normally through RAS with limited water exchange. The RAS meet the European Union's objectives for sustainable aquaculture, through food production and maintaining natural resources with minimal ecological impact [4]. However, RAS are complex systems in which fishes biomass and water chemistry/quality interact and, therefore, small variations can lead to non-ideal conditions, inducing

stress, reducing food intake and growth performance, or, due to high acute or chronic stress, can even conduct to mortality [5].

Therefore, critical parameters like plasma cortisol need to be monitored to ensure fish well-being. The traditional way to measure cortisol in fishes is through blood sampling and blood plasma analysis, however, this is an invasive method in which the results can be doubtful due to the stress caused by the sampling method. In addition, the sampling method is time-consuming, and many times uses anesthesia protocol to collect samples. The waiting time to get results is also too long [28], [29].

Later, it was demonstrated for some fish an increase in the release rate of cortisol into the water in response to stress, and also that this phenomenon was correlated with plasma cortisol concentrations, in which the cortisol concentrations in water were significantly higher in groups with a high fish density (~3.084 ng/mL) than in groups with low density, due to the greater fish biomass [28], [29]. Usually, liquid chromatography-tandem mass spectrometry (LC-MS/MS), utilized in analysis laboratories, is used to measure cortisol levels. Nonetheless, the monitoring of fish stress in POC and the controlling of water quality are the key points for fish production with quality and promotion of fish well-being.

This means that it is crucial the development of technology that offers socially, scientifically, and financially countless benefits in these areas, to be exact, devices that allow stress monitoring in real-time, cost-effective, and in a non-invasive way.

2.2 Cortisol Biosensors in Medical and Biological Applications

The last three decades have witnessed enormous activity in the field of biosensors. The reason for this to happen is not only related to the high sensitivity, precision, and speed of the detection mechanism of biosensors but also due to the low instrumentation needs and great technical simplicity in taking measurements [30]. All these characteristics make biosensors a favorable and suitable tool for POC.

Biosensors are analytical devices that convert a biological response into an electric signal, which use a live component or biomolecule, as the biorecognition element, immobilized onto the surface of a transducer (physicochemical detector component) [31]. In this way, when a target analyte interacts with the biorecognition element, physicochemical changes occur on the transducer surface and are recognized. Then, such changes are converted into measurable signals [31]. These devices should be highly specific, independent of physical parameters, like pH and temperature, and if possible, they should be reusable.

Biosensors can be classified in several ways: based on the biorecognition component used; based on the type of transducer; or based on the interactions between analytes and the biorecognition element [31].

The first point refers to enzymes, ABs, nucleic acids, cells, or microorganisms as the biological element [32]. The second point corresponds to a biosensor classification as magnetic, thermal, piezoelectric, electrochemical, or optical [33]. The third point refers to a classification of two classes: catalytic biosensor and affinity biosensor. In the former, a new biochemical reaction product is formed on the surface of the transducer due to the interactions, and the steady-state concentration is measured by this kinetic device, in which the biocatalyst used can include enzymes, microorganisms, organelles, or tissue samples [31], [34]. In the latter, physicochemical

changes to the transducer surface are measured, owing to irreversible binding between receptor molecules and the analyte that occur as a result of interactions. In this case, ABs, nucleic acids, or hormone receptors work as receptor molecules [31], [34].

Several studies with biosensors have been conducted to detect cortisol. For instance, in 2008, Richard C. Stevens *et al.* [35] developed a portable SPR biosensor system to detect cortisol in saliva. In this study, it was produced a competitive assay with cortisol-specific monoclonal ABs combined with a specially designed flow cell and used a six-channel portable SPR biosensor incorporated with three-channel Texas Instruments Spreeta 2000 sensing chips with gold surfaces. When testing this biosensor in laboratory buffers, the LOD was 0.36 ng/mL, whereas in saliva the value was 1.0 ng/mL. This last detection limit was considered by the investigators as sufficiently sensitive for clinical use.

P. Usha *et al.* [3], in 2017, proceeded with an innovative study using an optical fiber biosensor also for cortisol detection in saliva, however, in this research was used a contemporary approach of lossy mode resonance and molecular imprinting of nanocomposites of ZnO and polypyrrole. The sensor production was accomplished by uncladding a polymeric-clad silica fiber in the middle and coating that zone with ZnO film. Afterward, the ZnO film was coated with a polymeric film to later form a molecular imprinting polymer layer. The LOD calculated was 25.9 fg/mL.

Another study for cortisol detection in human saliva was conducted in 2020 by Seongjae Jo *et al.* [36]. Researchers chose to use gold nanoparticles in order to fabricate a localized surface plasmon resonance (LSPR) sensor with an aptamer immobilized on AuNP substrate. This aptasensor was able to detect cortisol in a range from 0.1-1000 nM with a detection limit of 0.1 nM. This aptasensor was also tested for cortisol detection with other substances with similar chemical structures to prove its selectivity and was succeeded.

This year, Cátia Leitão *et al.* [8] produced an SPR tilted fiber Bragg grating (TFBG) immunosensor for cortisol detection. To develop this sensor was used a standard silica telecommunication single-mode optical fiber, in which TFBGs were engraved 1 cm long. The fiber was coated with gold and, then, functionalized with anti-cortisol ABs. As the interrogation method, it was practiced an alternative to the usual, it was signalized the local maximum of the plasmonic signature of the lower envelope to monitor the SPR mode. As a result, the attained sensitivity was 0.275 ± 0.028 nm/ng.mL^{-1} for a linear concentration range of 0.1-10 ng.mL^{-1}.

In another 2021 study, Cátia Leitão *et al.* [7] used a POF coated with AuPd alloy and functionalized with anti-cortisol ABs to develop an SPR immunosensor for cortisol detection. Through the RI variation on the AuPd surface, due to AB-antigen binding, it was calculated the SPR wavelength shift. Therefore, 3.56 ± 0.20 nm/log(ng/mL) was the sensitivity obtained with a LOD of 1 pg/mL. Furthermore, it was performed selectivity tests in a sensor functionalized with ABs for human chorionic gonadotropin (anti-hCG ABs). These tests were well succeeded since the SPR wavelength shift was not significant.

Although all these mentioned studies have used optical biosensors, many investigations have also been conducted for cortisol detection with electrochemical biosensors. For example, in 2008 Ke Sun *et al.* [37] functionalized microfabricated Au electrodes encased in a microfluidic chamber to fabricate a sandwich structure. In this way, anti-cortisol ABs were immobilized on electrodes followed by cortisol antigen immobilization and attachment of detector AB with alkaline phosphatase (AP). Consequently, an immunoelectrochemical sensor based on AP enzyme for the determination of salivary cortisol concentration was fabricated.

In 2017, Yo-Han Kim *et al.* [38] reported a chemiresistor GO sensor for cortisol detection. For that, GO was coated and reduced on an indium-tin-oxide glass surface followed by cortisol

monoclonal AB immobilization. The detection method used was based on the resistance change of the rGO chemiresistor. The attained LOD was 10 pg/mL.

In the same year, Kwang Su Kim *et al.* [39] reported a novel electrochemical biosensor for cortisol detection, in which the electrochemical sensing platform consisted of an rGO electrode functionalized with denatured bovine serum albumin (BSA) protein layer and anti-cortisol AB probes. This impedimetric cortisol biosensor showed a LOD of 10 pM.

Many approaches have been employed for cortisol detection, especially electrochemical and optical biosensors. However, the focus of this dissertation will be on optical immunosensors, which are biosensors that comprehend ABs as receptor molecules. This type of biosensor is part of the class of affinity biosensors [40] and has been extensively investigated and developed for various applications, due to its advantages in terms of high specificity and selectivity when an immunoreaction, AB-antigen binding arises. Summarily, ABs can specifically recognize and bind to the corresponding antigens forming a stable immunocomplex [40].

Going into more detail about immunosensors, these can be nominated label-free or labelled immunosensors. The former has that designation since the physical changes in the transducer caused by AB-antigen binding are directly measured, allowing the detection of the immunocomplex formation. The latter is developed incorporating a sensitively detectable label, in which the label is measured to detect the immunocomplex formation [41]. Some of the labels used can be radioisotopes, chromophores, fluorophores, or enzymes [40].

Optical biosensors offer long-distance detection, electromagnetic immunity [42], among others, and the basic purpose is to produce a signal proportional to the concentration of a measured substance (analyte). Optical detection is performed by exploring the interaction of the optical field with a biorecognition element [33].

To summarize, although many and different biosensors have been developed for cortisol biosensing, this area is an ongoing challenge to achieve the best sensor material, the best performance and physical structural miniaturization, and the best low-cost configuration for particular scenarios. Therefore, it is crucial to continue with the investigation, production, and improvement of this technology so that, in a near future, it can be applied in POC.

2.3 Optical Fiber Biosensors

The huge interest in optical fibers as a data transmission system started in 1960 when the laser was invented. Optical fibers emerged to become the most important transmission medium, and revolutionized modern communications and optical science. Researchers were encouraged to study the use of optical fiber for data communication, sensing, and other applications when they realized the capability of the laser systems to send a very large amount of data compared to microwaves. In this way, the fast development and continuous improvement of optical fiber technology prompted researchers to create sensors with optical fibers, combining optical fiber telecommunications with optoelectronic devices [43]. In the mid-1960s was patented the first optical fiber sensor. After ten years, researchers developed the first optical fiber sensor due to the appearance of the first single-mode optical fiber which was integrated into interferometers. Later in the 80s, an optical fiber gyroscope was commercialized and became one of the first applications of optical fiber sensors, which started to be a crucial component in stabilization and navigation systems. Approximately a decade later, several types of optical fiber sensors started to be implemented in the civil industry to

measure different physical parameters, such as strain, temperature, pressure, among others. FBGs also started to be experimented and, around 2000, FBG based sensors began to be used in civil industry applications [44]. This is an ongoing area since many different types of optical fiber sensors continued and are still being invented and studied in order to improve these devices for several applications.

The basic structure of an optical fiber biosensor system consists of an optical source, a transducer, and a receptor. The optical source is usually a laser, diode, or LEDs. The transducer element is an optical fiber, which can also be composed of other biocompatible and biofunctional materials/structures. In the receptor, there is a photodetector that is used to detect changes in the optical signal caused by the disturbance of the system with the variable to be measured [43].

Optical fiber sensors are capable to adapt to adverse environmental conditions [43] and have other advantages, such as relatively small size that allows its integration in areas where other sensing methods are difficult to implement, electromagnetic interference immunity, corrosion resistance, the possibility of multiplexing several sensors in the same optical fiber, among others [45]. For those reasons, they have become an indispensable option in various applications, including civil, mechanical, electrical, aerospace, automotive, nuclear, medical, and chemical engineering [43]. As in all techniques, optical fiber sensors also have some drawbacks, for instance, possible interference with the guided light on the fiber caused by fluorescent species or by species that absorb in certain spectral regions, and fragility since the fiber can break if it is tightly bent.

An optical fiber is a circular structure with a central core surrounded by cladding and a protective layer, in which total internal reflection (TIR) phenomenon occurs when light enters the fiber, due to the difference between the RI of cladding and core, in which the core RI is superior to that of the cladding. Therefore, if a light beam hits the cladding with an angle inferior to the critical angle (angle of incidence where the angle of refraction is 90º), the beam is refracted. However, if the angle is superior, the beam is reflected, and TIR happens [43], [45].

Optical fibers can be distinguished by the number of modes that can be transmitted. This means that, when the light propagates inside the optical fiber as an electromagnetic wave in single-mode, the fiber is designated single-mode fiber (SMF), and when the propagation takes place in several modes, is designated multimode fiber (MMF). Depending on the diameter of the optical fiber and the wavelength of the radiation, the number of modes that can propagate through the core changes. Optical fibers with a minor core only allow a single mode, but fibers with a larger core allow multiple modes [45].

In addition, optical fibers can be fabricated with different materials: SOFs, which were the first fibers to be used in the field of biosensing and continue to be the most widely used; and POFs, which appeared later owing to recent advances in polymeric optical fiber technology. The POF core is made of poly(methylmethacrylate) (PMMA) with a fluorinated polymer cladding [46].

Depending on the application, optical fiber sensors can be constituted from SMF or MMF [45]. In biosensors are usually used SOF SMFs or POF MMFs, since the core radius of SOF is much inferior compared to commercial POF. The cladding and core diameter of a SOF SMF is ~125 μm and ~9 μm [47], respectively, while POF MMF has a total diameter of 1000 μm and a core diameter of 980 μm with a cladding thickness of 10 μm [48].

2.3.1 Biosensing Principles

2.3.1.1 Evanescent Wave

As aforementioned, light propagates in the fiber core through the TIR phenomenon, where the light transits through successive reflections on the core-cladding interface practically lossless. Nonetheless, during TIR some light extends beyond the core to the surrounding cladding. This phenomenon is known as the EW and can be used as an interrogation method in biosensing [49]. Summarily, there are the guided field in the core (core modes) and the evanescent field in the cladding (cladding modes) once light propagates in the optical fiber [50]. The only contributing rays for the evanescent field are the ones that strike the interface core-cladding with angles near the critical angle [49]. Moreover, the evanescent field decays exponentially to zero with increasing distance to the core before reaching the external medium, and the short distance in which the field decreases to 1/e of its initial value at the interface is designated penetration depth [49], [50]. The discovery of this phenomenon was and still is very important in biosensing since it is possible to detect analytes through the interaction of the EW with those analytes in the penetration depth [34]. Most different optical fiber biosensor configurations, like D-shape, unclad, tapered, U-shape fibers, long-period gratings (LPGs), and TFBGs, use EW-based transducer mechanisms [8].

2.3.1.2 Surface Plasmon Resonance

SPR is one of the optical methods that has been used the most in optical fiber biosensing since it was introduced in 1993 by Liedberg et al. [51]. This technique is sensitive to small changes of the RI on the fiber surface and enjoys the advantages of high real-time response rate, high sensitivity, low LOD, and allows label-free monitoring of biomolecular interactions, leading it to be widely applied in biosensors and in the field of *in situ* biomedicine [52], [53].

As mentioned before, an EW is created when light travels from one medium with higher RI to a medium with lower RI. This EW penetrates and is enhanced when a metal film is placed at the interface of the mediums [54]. As a result of the EW penetration, electrons in the metal surface layer are excited [55]. Therefore, at the interface between the two mediums are generated quantized collective oscillations of free electrons, which are categorized as SPs [50], [52]. When these SPs are excited by photons of the incident light, surface waves at the metal-dielectric interface (surface plasmon polariton (SPP)) are generated, in which its propagation is confined to the referred interface [54], [55]. Under the resonance condition, the EW can excite the SPs, creating a phenomenon called SPR [54]. Resonance condition happens when the incident light and the SPs have equal propagation constants, leading to momentum matching and, therefore, resonance [52]. A slight variation in the refractive index of the medium leads to a change in the SPR propagation constant and, in turn, to a spectral change. In this way, a displacement of the resonance position or the intensity modification can be used as the interrogation method to detect small changes in the RI, which makes this phenomenon a good option for biosensing [42]. It should be noted that SPs are composed with only an electric field component normal to the surface. As a result, SP waves are polarized (transverse waves) having an oscillating electric field also normal to the surface. Therefore, the incident light must be polarized to trigger SPR. [56].

The first SPR sensor was based on a prism and was presented by Otto in 1968 [57] (**Figure 2-a**). In this first configuration, the analyte layer was placed between the prism and the metal layer [58]. In this case, after the light is injected in the prism with an incidence angle greater than the critical angle, TIR takes place inside it and an EW at the prism-analyte layer interface is created, which can excite SPs at the analyte layer-metal interface, and SPR is generated. However, this configuration had a problem, the SPR efficiency was reduced since EW decays with distance [52]. Later the Otto configuration was upgraded by Kretschmann (**Figure 2-b**), in which a metal layer was placed between the prism and the analyte layer [58]. With this new configuration, the propagation of the EW was enhanced, allowing the transference of energy to SPs under the resonance condition. As a result, the SPR phenomenon is achieved [52].

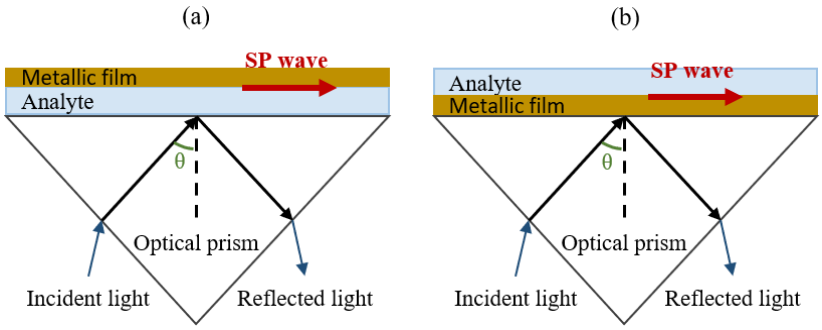

Figure 2 - (a) Otto configuration, (b) Kretschmann configuration.

Based on the similar sensing principle, coupling SPR to optical fiber technology has brought enormous advances, offering attractive advantages over traditional prism-based SPR platforms such as simplicity, cost-effectiveness, and miniaturization [42]. Currently, optical sensors based on SPR can be found in different applications in life sciences, electrochemistry, environmental safety, and biomedical diagnostics [52]. To improve the performance of optical fiber sensors based on SPR, many efforts have been made until now.

Therefore, along with several optical fiber structures, such as uncladded, D-shaped, U-shaped, tapered, end-face reflected, grating-modified, different plasmonic materials have also been deposited onto these structures and studied to further improve sensitivity [42].

The metallic film is one important factor that affects the performance of an SPR biosensor, with Au, copper (Cu), Ag, and aluminum (Al) the most commonly used. Nonetheless, Au is the most applicable metal since has more favorable advantages, such as low valence energy band, stable chemical properties and provides the highest sensitivity, which makes it suitable as a plasmonic material for biosensors [59]. The metal nanofilm thickness is an important characteristic that needs to be considered when depositing Au on the optical fiber sensor surface. For instance, 50 nm is the Au thickness that allows a higher sensitivity of the sensor, since with this thickness it is possible to acquire the narrowest and deepest SPR attenuation [60]. Nonetheless, a very small variation in Au thickness (for instance, 5 nm) at the time of deposition can cause a change in SPR wavelength position, affecting sensors' sensitivity and, consequently, sensors' performance [61].

2D materials have also been studied over the years as substitutes for metallic films or applied together with them, to further improve biosensor performance. These materials have atomic thickness resulting in exquisite optical, electrical, mechanical, structural, and chemical properties. The properties that stand out the most are the optical, such as universal optical conductivity, broadband absorption from visible to infrared frequency, and novel gate-tunable plasmonic properties [62].

Graphene is one of the materials that started being used more in optical fiber biosensors. Graphene has a hexagonal lattice structure constituted with carbon (C) atoms, which allow him to have a high specific surface area (2630 m^2g^{-1}) [63], high carrier mobility (250 000 $cm^2V^{-1}s^{-1}$) [64], thermal conductivity (about 3000 $Wm^{-1}K^{-1}$) [65] and high transmittance (visible light and near-infrared light absorption 2,3 %) [66]. Further, it contains excellent mechanical properties (Young's modulus of 1×10^{12} Pa) [63], good chemical stability, and biocompatibility [67]. These unique properties make graphene suitable for many applications, including in plasmonic optical fiber biosensors. In this case, when graphene layers are deposited on the metal layers, a strong coupling at the graphene/metal interface can be induced, in which electrons from graphene are transferred to Au, promoting electrons collective resonance on the Au surface. As a result, the electric field and sensitivity are improved. In addition, owing to graphene's delocalized π orbitals and good biocompatibility, molecule adsorption capacity and stability of biosensors are enhanced [42], [59].
Other materials, such as GO [68], molybdenum disulfide (MoS_2) [69], ZnO [70], among others, have also been extensively used in this field. However, the use of these materials is recent and there are not many investigations that prove their performance, thus, further studies are required.

2.3.2 Designs

As already mentioned, light propagates inside the optical fibers through the TIR phenomenon, which occurs with virtually no losses to the surrounding (cladding). This is a problem because limits the interaction of light with the analytes of interest that are intended to be the measure [50]. Consequently, researchers started to study and fabricate new optical fiber configurations to produce biosensors with enhanced performance, in which the interaction of light with analytes is possible. The most common designs that have been studied consist of geometry-modified structures where the cladding is entirely or in part removed via chemical etching process, by side-polishing, or micromachining using femtosecond or ultraviolet (UV) laser [71]. Further, grating-assisted fibers have also been proposed for biosensing.

2.3.2.1 Geometry-Modified

Until now, many different geometry-modified sensing structures have been studied to develop optical fiber biosensors, including D-shaped, uncladded, tapered, U-shaped, and end-face reflected.

D-shaped sensing structures are created removing part of the cladding on one side of the optical fiber as can be seen in **Figure 3-a**. Therefore, is created a flat side-wall that allows direct interaction of the EW with the metallic film coated on a D-shape surface leading to the SPR phenomenon [72]. The operating wavelengths, which most D-shape optical fiber biosensors use, range from 500 to 800 nm [71].

The process of developing an unclad or etched structure (**Figure 3-b**) is similar to that of the D-shaped, but in this case, the cladding removal is practiced all around and in one area of the optical fiber [58]. As a result, EW can directly interact with the metal coated on the etched region, allowing the triggering of SPR, as well as with the analytes layer deposited on the metal surface. The operating wavelengths obtained with this structure are the same as the D-shape configuration.

Figure 3-c shows another configuration used in sensors that consist of tapered fibers. To perform tapered structures is used a flame or heated filament to heat the fiber while is stretched

along the propagation axis [71]. This method can be performed in fibers in which the cladding was removed first, or in fibers with both core and cladding placed [73]. In both cases, the diameter of the core and/or cladding of the fiber decrease a few millimeters, and the central region of the fiber gets more thinner [71]. When light guided in the core reaches the tapered area, part of that light leaks to the surrounding medium [58]. Afterward, this EW can interact with a metallic film coated over the tapered section, hence, SPR is promoted, and sensitivity is enhanced. 12000 nm/RIU is the ultimate refractometric sensitivity reached by this structure [71].

When an optical fiber is bent beyond a certain critical radius forming a U-shape structure (**Figure 3-d**), the light losses become more evident. This event can be used with metallic films to produce optical fiber biosensors based on SPR, since the EW becomes more radiative in this case, in other words, is enhanced [58], [71] due to the coupling between the core mode and the cladding modes. To fabricate this structure usually is used a flame to heat a section of the fiber while is flexed. Flexing the fiber without a heat source would create very strong tensile stresses [71].

The last sensing structure is called end-face reflected (**Figure 3-e**), since in this configuration the light is reflected at the end of the fiber, in contrast to the structures described above that are all transmission. To allow reflection at the end of the fiber, the cladding of that area is removed and, later, a reflective material is added. The optical path doubles when light is reflected in the reflective layer and reaches again the incident point, increasing the SPR effect and sensitivity. The end of this structure can be flat or inclined, thus, there are three designations for this configuration: flat tip, tapered tip, or angle polished tip [58].

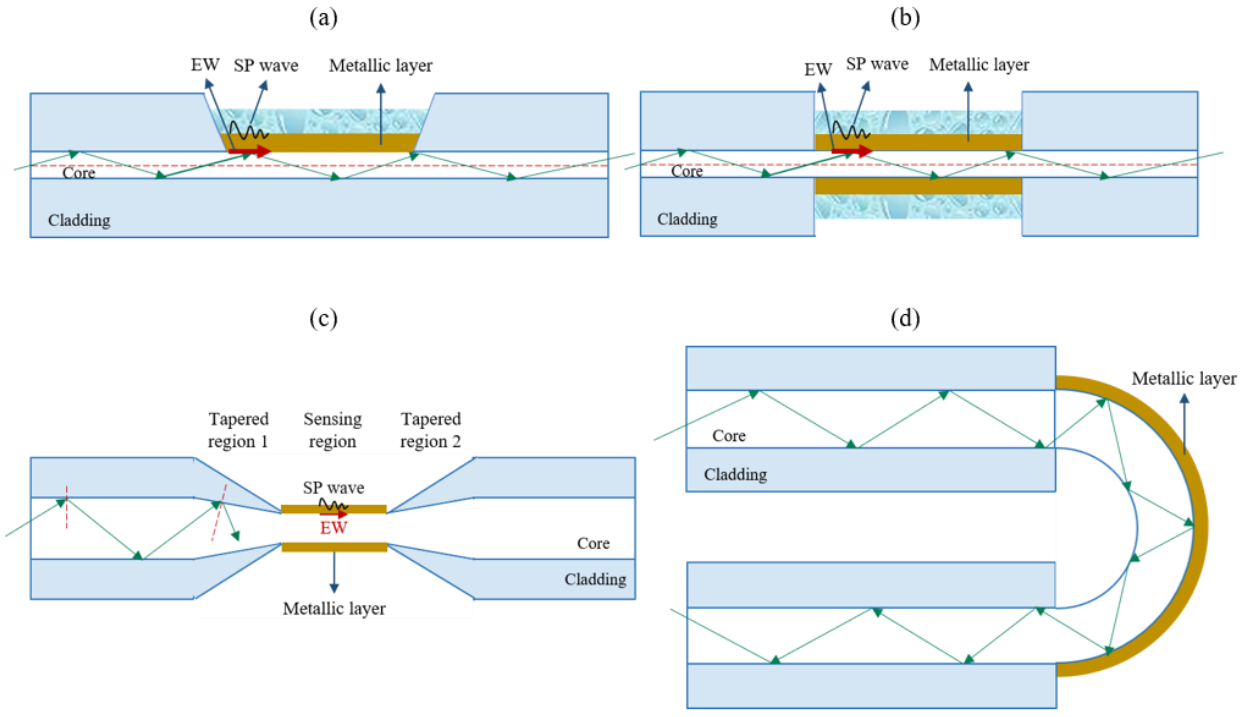

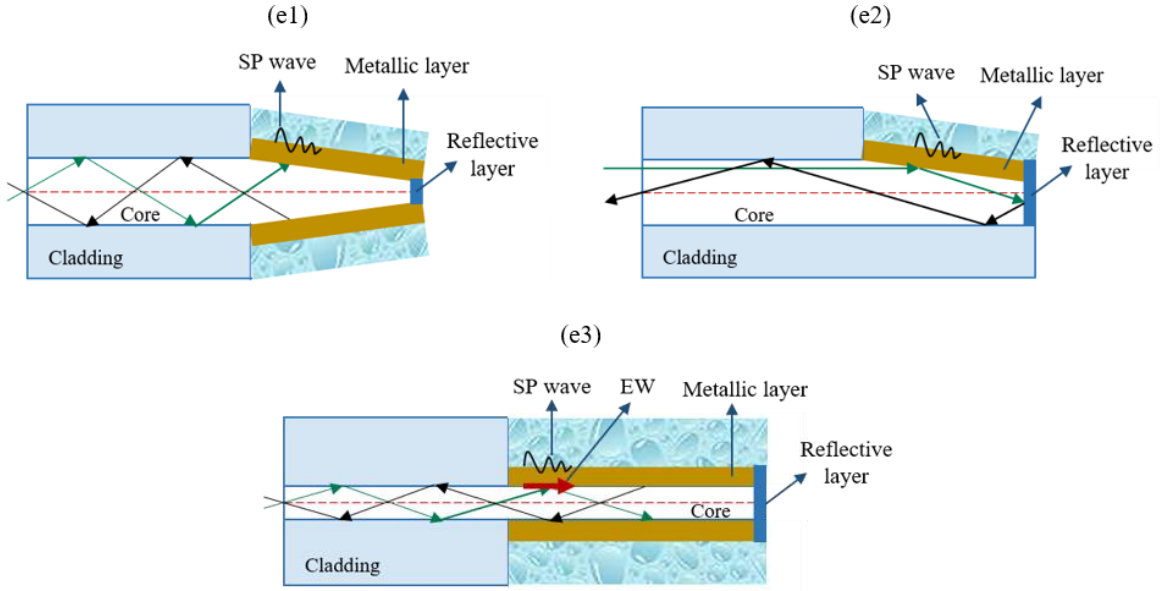

Figure 3 - (a) D-shape, (b) Unclad, (c) Tapered, (d) U-shape, (e) End-face reflected – (e1) tapered tip, (e2) angle polished, and (e3) flat tip sensing structures.

2.3.2.2 Grating-Assisted Fibers

Fiber gratings consist of periodic or aperiodic perturbations of the RI of the core. Within the first case, fiber gratings can be divided into short-period fiber gratings or fiber Bragg gratings (FBGs) where TFBGs are included, and LPG. In case of fiber gratings with aperiodic perturbations, in which the period varies along the grating length, usually, the RI of the core, are classified as chirped FBGs (CFBGs) [50], [52]. Summarily, FBG contains a period in the order of 500 nm, while, an LPG has a grating period on the order of 100 micrometers, to a millimeter [50]. In a CFBG the period is similar to that of FBG, however, in this case, the period increases along its length.

FBGs were demonstrated by Ken Hill in 1978 [74]. Initially, gratings were manufactured using a visible laser whose light propagated inside the fiber core. Later, Gerald Meltz et al. in 1989 demonstrated a more flexible technique in which the core was exposed to UV laser lighting through the cladding, designated transverse holographic inscription [75]. The periodic structure of the Bragg grating in the fiber was created using the interference pattern of the UV laser. After years of FBGs quick development, laser inscription techniques have also evolved and currently is possible to inscribe gratings with high quality through femtosecond laser systems [76], [77].

As shown in **Figure 4**, in FBGs is accomplished a coupling between the fundamental core mode and its respective counter-propagating mode [50]. In this way, FBGs are based on the action of narrowband reflectors, in which the grating pitch determines the light wavelength that is reflected. Periodic disturbances in FBG-based sensors essentially act as wavelength filters, since only a specific wavelength experiences constructive interference whereas many wavelengths reflected at each perturbation disappear by destructive interference with other reflected signals. According to phase-matching condition, the coupling only happens for one specific wavelength, the central wavelength known as Bragg wavelength, described as [73]:

$$\lambda_B = 2n_{eff}\Lambda \quad (1)$$

Where λ_B is the Bragg wavelength or reflected peak, n_{eff} is the effective RI of FBG, and Λ is the grating period.

Summarily, the operation principle of an FBG is based on the dependence of Bragg wavelength on the effective RI and grating period.

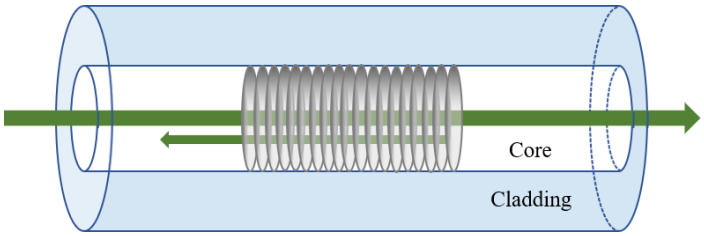

Figure 4 - Uniform FBG and light mode coupling (propagation direction indicated by the green arrow).

In standard FBGs, the light cannot reach the cladding since its propagation is firmly confined within the core [50], therefore, coupling only happens between core modes [58]. Consequently, the external RI does not influence the effective RI, hence, the sensitivity to the external RI is practically none [50], [78].

Nonetheless, the transmitted light confined in the core will be influenced by the external RI if the FBG cladding is totally or partially removed along the grating area by the etching process [58], [78]. Besides the etching process, cladding reduction can be accomplished by other techniques, such as grinding, or fine-drawing-cone [58]. As a direct consequence of the geometric modification, changes in Bragg wavelength combined with reflection amplitude modulation can occur owing to the external RI influence on the effective RI [78]. With this new structure, etched FBGs can be used in biosensing since can detect changes in the measurand. In 2001, Kumazaki et al. used etched FBGs for the first time to develop a tunable wavelength filter [79].

As in common FBGs, TFBGs (**Figure 5-a**) also exhibit a periodic modulation of RI along the fiber axis, however, the gratings are uniformly tilted by an angle θ between the grating plane and the grating transverse section less than 45° [80], [81]. Consequently, besides the coupling between core modes, there is also the coupling between core modes and cladding modes, including the coupling between the core mode and the counter-propagating cladding mode, and between the core mode and the radiation mode [80]. Depending on the tilt angle, the coupled light can have different directions. In this way, the typical transmission spectrum (**Figure 5-b**) has many resonance peaks (narrow attenuation bands), corresponding to different coupled cladding modes. That figure shows two transmission spectra of a TFBG, one referring to the P polarization mode and the other to the S polarization mode of the incident light [82], with the polarization state as a key point in this type of FBG. The SPR phenomenon is very sensitive to the polarization state. Therefore, as the SP waves are P polarized, it is desirable to have an incident light also P polarized, and not S polarized, to ensure a more efficient excitation of the SP waves and, consequently, obtain a more evident SPR phenomenon [83].

The Bragg condition of a TFBG takes into account the resonance wavelengths of the several cladding modes [50]:

$$\lambda_{res(m)}^{TFBG} = \left(n_{eff}^{core} - n_{eff}^{clad(m)}\right)\frac{\Lambda}{\cos(\theta)} \quad (2)$$

where n_{eff}^{core} is the effective RI of the core and $n_{eff}^{clad(m)}$ the effective RI of the m^{th} cladding mode. In this case, the maximum sensitivity is attained when the cladding effective RIs are similar to the surrounding RI [58]. Moreover, exists a shift in the resonance wavelengths of the corresponding cladding modes to longer values when the surrounding RI increases [81]. The first TFBG sensor for surrounding RI detection was accomplished by Laffont and Ferdinand in 2001 [84]. Years later, Yanina Y. Shevchenko and Jacques Albert reported the first TFBG SPR sensor in 2007 [85].

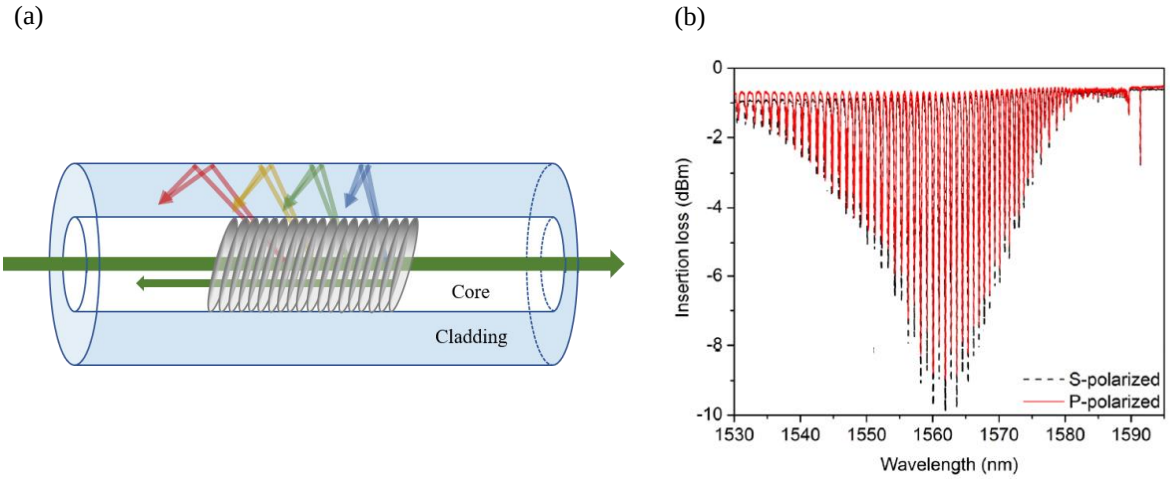

Figure 5 - (a) TFBG and respective light mode coupling, (b) TFBG transmission spectra under P and S polarization [82].

In contrast to TFBGs, in LPGs (**Figure 6**) the period extends to an order of a fraction of a millimeter and allows the coupling of the guided mode light (fundamental core mode) to the co-propagating cladding modes [50], [86]. As a result of the coupling, the transmission spectrum of an LPG presents several attenuation bands corresponding to resonance peaks related to the coupling of several cladding modes. This means that the resonance wavelength for the m^{th} cladding mode is given by [50]:

$$\lambda_{res(m)}^{LPG} = (n_{eff}^{core} - n_{eff}^{clad(m)})\Lambda \quad (3)$$

In this case, the cladding modes are sensitive to changes in the surrounding RI. In contrast to TFBGs, if the surrounding RI increases, a shift to lower resonance wavelength values occurs [81].

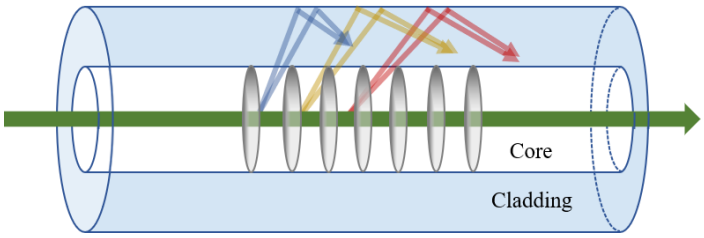

Figure 6 - LPG and respective light mode coupling.

III - Simulation

This section is reserved for the description of the plasmonic D-shape SOF and POF sensors simulation that was carried out throughout this work. Therefore, a brief explanation of the steps taken to simulate these sensors will be presented as well as a theoretical foundation. Subsequently, the achieved results will be shown and discussed.

3.1 D-shape SOF and POF Model

In order to simulate Au-coated D-shaped SOF and POF, it was used the COMSOL Multiphysics software package. In this software, it is possible to design different components in different dimensions, such as 3D, 2D, and 1D, symmetric or asymmetric. Besides, it is possible to reduce the number and size of the elements through the mesh. The use of 3D dimension requires a high processing time. Moreover, COMSOL software presents several modules with different tools for each module.

In this work, it was selected in the first place the Model Wizard 2D, since the mode analysis is accomplished on the cross-section in the *xy*-plane of the fiber with the wave propagating in *z* [42], and then, the RF module also known as electromagnetic waves frequency domain. Afterward, the geometry of the fiber was established creating two concentric circles representing cladding and core. In the case of SOF, the radius of the cladding and core were settled at 62.5 µm and 4.1 µm, respectively. In POF, the established radius for cladding and core was 500 µm and 490 µm, respectively.

Next, it was necessary to specify the RI of the core and cladding. As already known, the RI of the materials varies with wavelength due to the dispersion effects [87]. As a result, the RIs of the fiber were calculated through the Sellmeier equation, which is an empirical relationship between the RI and the wavelength for one specific transparent medium. The core of a SOF is doped with a fraction *X* of germanium (Ge) to generate a higher RI compared with the RI of the cladding. In this way, the Sellmeier equation for the core is given by [87]:

$$n = \sqrt{1 + \sum_{j=1}^{3} \frac{[A_j + X(GA_j - A_j)]\lambda^2}{\lambda^2 - [l_j + X(Gl_j - l_j)]^2}} \tag{4}$$

and the RI of the cladding, which is not dopped with Ge ($X = 0$), is presented by [87]:

$$n = \sqrt{1 + \sum_{j=1}^{3} \frac{A_j \lambda^2}{\lambda^2 - l_j^2}} \tag{5}$$

The fraction *X* of Ge is unknown, and to find this value was necessary to calculate the mode-field diameter (MFD). For that, several values of *X* were experimented until obtaining an MFD of 10.5 µm for 1550 nm (operating wavelength of an SMF-28). The selected fraction *X* of Ge

was 0.0305. To obtain the MFD, firstly the effective area was calculated through the following equation:

$$A_{eff} = \frac{\left(\iint_s |E_t|^2 \, dx \, dy\right)^2}{\iint_s |E_t|^4 \, dx \, dy} \tag{6}$$

where the $|E_t|$ is the modulus of the electric field attained through COMSOL. Finally, the MFD is determined using the calculated effective area through the following equation:

$$A_{eff} = \pi \frac{MFD^2}{4} \Leftrightarrow MFD = \sqrt{\frac{4A_{eff}}{\pi}} \tag{7}$$

Regarding POF, the core is constituted with PMMA and the cladding is made of a fluorinated polymer polyhexafluoro isopropyl 2-fluoroacrylate (PHFIP 2-FA). As a result, the RI of the core and cladding are given by the aforementioned equation 5. The different Sellmeier coefficients for both core and cladding of SOF [87] and POF [88] are presented in **Table 1**.

Table 1 - Sellmeier coefficients for SiO_2, GeO_2, PMMA, and PHFIP2-FA.

		j	1	2	3
SOF	SiO_2	A_j	0.69616630	0.40794260	0.89747940
		l_j	0.06840430	0.11624140	9.89616100
	GeO_2	GA_j	0.80686642	0.71815848	0.85416831
		Gl_j	0.06897260	0.15396605	11.8419310
POF	PMMA	A_j	0.4963	0.6965	0.3223
		l_j	0.0718	0.1174	9.2370
	PHFIP2-FA	A_j	0.4200	0.0461	0.3484
		l_j	0.0587	0.0878	0.0927

In the case of SOF, using these coefficients and the aforementioned parameters, it was possible to determine $|E_t|^2$ and $|E_t|^4$ for MDF calculation. Thus, in COMSOL the *Step I: Mode Analysis* in *Study* option was selected and the modes were searched around the RI of the core. Then, the *Compute* option was selected and results were obtained, allowing the calculation of the $|E_t|^2$ and $|E_t|^4$ using the Surface Integration option.

Before these steps, was necessary to create a mesh for both SOF and POF, which is the division of the principal domain into smaller subdomains with different sizes. The smaller are present near the interfaces between different mediums. This happens to compensate for the accentuated variations in the electromagnetic field.

After this process, a D-shape structure was designed in SOF and POF. For that, in SOF, part of the cladding circle was cut to the core, leaving a cladding thickness of 0 µm. In the case of POF, not only the cladding circle was cut but also the core circle, since the cladding thickness is only 10 µm. The cut was performed at 300 µm from the fiber center. In both cases, an Au layer was created

in the D-shape zone with a thickness of 50 nm and 60 nm, respectively. All the mentioned parameters were inserted according to the fibers that were used in the experimental trials.

To determine the RI of the dielectric material, it was used a COMSOL library, Johnson and Christy 1972 [89], which is the most applied in optical fiber simulation.

In order to characterize the SOF and POF immunosensors to the external RI, a circular structure was created around the D-shape structure with a radius of 63 µm and 505 µm, respectively. In this layer, eight different RI values were inserted, such as 1.333, 1.334, 1.340, 1.346, 1.358, 1.368, 1.377, and 1.386, corresponding to glucose concentrations with 0, 1, 5, 10, 20, 30, 40, 50 % (w/v). To allow the formation of transmission spectra as a function of wavelength for each RI, it was necessary to obtain several complex modes for each wavelength in order to select the mode corresponding to the SPR. Therefore, in *Step I: Mode Analysis*, the modes were searched around the RI of the core and the desired number of modes was 35. Furthermore, in the *Study* option was selected a *Parametric Sweep* ranging from 570 to 760 nm to allow the determination of cladding and core RIs, as well as, the effective RIs of complex modes depending on the wavelength.

Afterward, using the imaginary part of the effective RI of the complex modes, it was calculated the transmission spectra. In case of POF, it was not possible to obtain the transmission spectra since no complex modes were attained.

In more detail, when a P-polarized light strikes a metal-coated fiber, SPs can be excited and a phase-matching condition can occur between the core mode and the plasmonic mode [42]. The light which propagates in the *z*-direction inside the fiber is an electromagnetic wave with an electric and magnetic field. These electromagnetic fields expressed in cylindrical coordinates are represented by [90]:

$$\tilde{E} = E(r,\theta)e^{j(\omega t-\beta z)} \quad (8)$$

$$\tilde{H} = H(r,\theta)e^{j(\omega t-\beta z)} \quad (9)$$

where E(r,θ) and H(r,θ) correspond to the field distributions in the fiber straight section, which can be obtained through the COMSOL. If no disturbances occur, these distributions always remain the same along the fiber. The exponential $e^{j(\omega t-\beta z)}$ is the undulatory part and is similar to the plane zone $Ae^{j(\omega t-kz)}$ of a plane wave equation, in which ω is the frequency and β is the propagation constant that equals the k of the plane wave given by:

$$k = nk_0, \quad (10)$$

where k is the wavenumber in a given medium, n is the RI of the material, and k_0 is the wavenumber in vacuum such that $c = \omega/k_0$.

In this way, β is also given by:

$$\beta = n_{eff}k_0, \quad (11)$$

where n_{eff} is the effective RI of modes. In the core modes, $n_{cladding} < n_{eff} < n_{core}$, and in the cladding modes, $n_{exterior} < n_{eff} < n_{cladding}$. The core modes were the modes attained through COMSOL to get the transmission spectrum.

All materials have losses, and if the materials that compose the fiber impose significant losses on light propagation, its RI must be complex:

$$n = n_R + in_I, \quad (12)$$

where n_R is the real part of RI and n_I is the imaginary part related to losses. In this case, n_{eff} must also be complex:

$$n_{eff} = n_{eff,R} + in_{eff,I} \quad (13)$$

Where β is also expressed as:

$$\beta = \beta_R + i\beta_I \tag{14}$$

It should be noted that when losses are small, as in the case of silica and PMMA, their RIs are not considered complex in the calculation of modes.

Taking into account the previous expression:

$$\tilde{\vec{E}} = \vec{E}(r,\theta)e^{i(\omega t-\beta z)} = \vec{E}(r,\theta)e^{i\omega t-i\beta_R z+\beta_I z} = \vec{E}(r,\theta)e^{\beta_I z}e^{i\omega t-i\beta_R z} \tag{15}$$

where, $e^{i\omega t-i\beta_R z}$ corresponds to the undulatory part, and $e^{\beta_I z}$ is related to losses, which is a decreasing exponential if $\beta_I < 0$.

Nonetheless, losses are generally measured in intensity (I) or power (P), expressed as:

$$I \text{ or } P \propto \left|\tilde{\vec{E}}\right|^2 = \left|\vec{E}(r,\theta)\right|^2 e^{2\beta_I z} = \left|\vec{E}(r,\theta)\right|^2 e^{-\alpha z}, \tag{16}$$

in which, $\alpha = -2\beta_I$ is the loss coefficient or attenuation constant.

Thus, the transmittance is given by:

$$T = \frac{P_{final}}{P_{initial}} = e^{-\alpha z} \tag{17}$$

To conclude, the mode analysis is performed on the cross-section in the xy-plane of the fiber, and to represent the mode propagation, the following equations can be used [42]:

$$\alpha = -2k_0 \mathrm{Im}\{n_{eff}\} = -\frac{4\pi}{\lambda_0}\mathrm{Im}\{n_{eff}\} \tag{18}$$

$$\beta = k_0 \mathrm{Re}\{n_{eff}\} = \frac{2\pi}{\lambda_0}\mathrm{Re}\{n_{eff}\} \tag{19}$$

where λ_0 is the wavelength. To produce the transmission spectra for each RI of glucose concentration, it was necessary to look for the mode that corresponded to the SPR, for each wavelength.

After exporting all the effective RIs of the modes, in MATLAB was created a routine that allowed the formation of the transmission spectra from the imaginary part of the complex modes through equation 17, in which z was considered the D-shape region length (10 mm).

3.2 Results and Discussion

Using the COMSOL software, it was possible to simulate the response of an Au-SOF sensor for different glucose concentrations using the respective RI values. In the case of Au-POF, was not possible to obtain such results. However, **Figure 7** shows the basic geometry implemented in both cases.

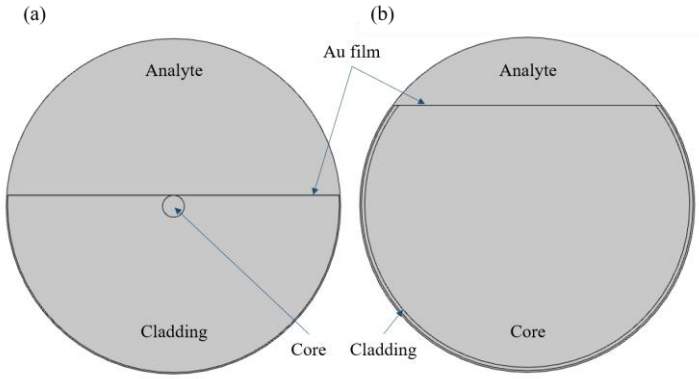

Figure 7 - Schematic diagram of models (a) Au-SOF and (b) Au-POF.

Through the Sellmeier equation and the respective coefficients, it was possible to obtain the RI of cladding and core of SOF and POF. RI versus wavelength plots are shown in **Figure 8**, in which is possible to verify that the core of POF (PMMA) presents a higher RI than the core of SOF (Ge-doped silica) in contrast to the cladding, in which the RI of silica is superior to the RI of PHFIP 2-FA. Thus, the difference between the RI of the core and the RI of the cladding of POF is greater than that of SOF. Anyway, it was confirmed that the RI of the core is superior to the RI of cladding, as expected, proving that no errors of this nature occurred in their calculation.

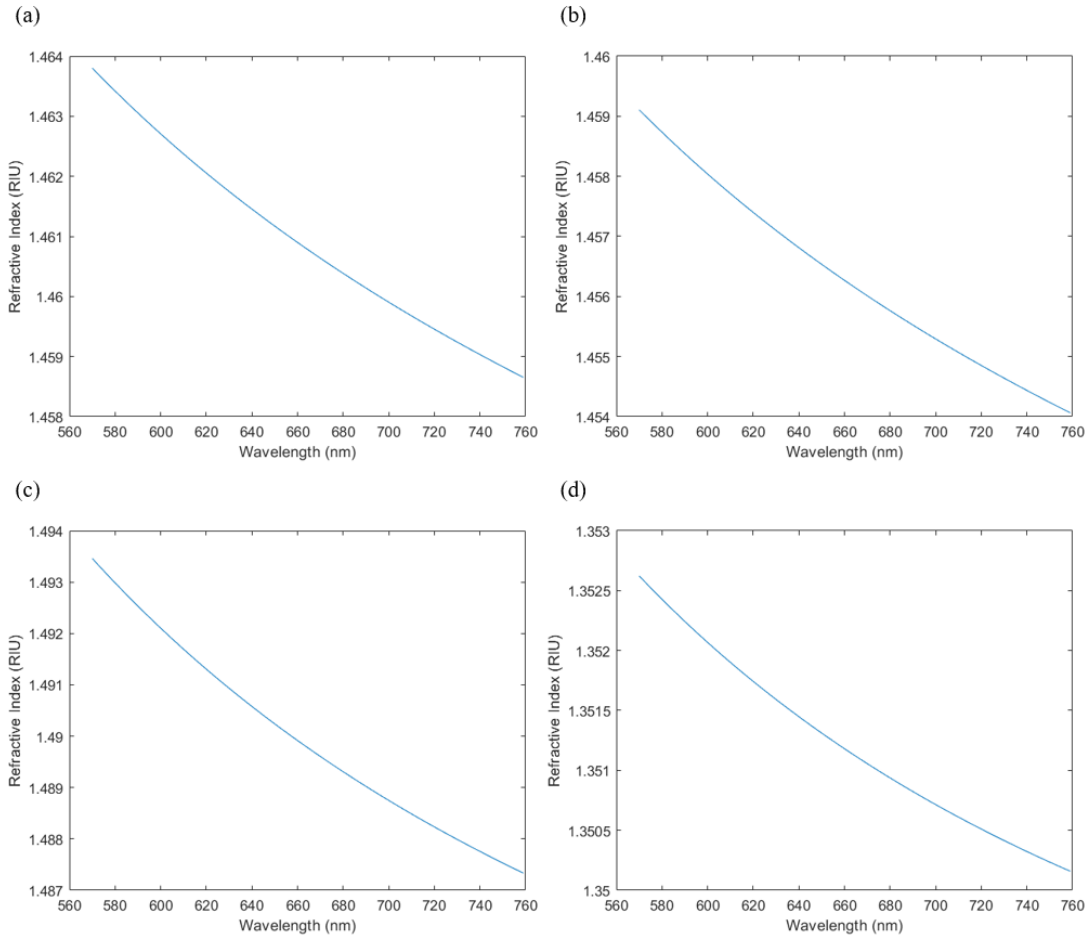

Figure 8 - Variation of (a) core RI and (b) cladding RI with wavelength in case of SOF; Variation of (c) core RI and (d) cladding RI with wavelength in case of POF.

To characterize the Au-SOF sensor based on SPR to the RI, it was necessary to choose the SPR core mode for each wavelength. **Figure 9-a** presents the mode profile corresponding to the SPR phenomenon. Besides, the wavelength interrogation method was employed to analyze the sensor response to different glucose concentrations. Thus, in **Figure 9-b** is possible to observe a continuous increase in the spectral wavelength with increasing RI. In order to calculate the sensitivity of the simulated sensor to RI, defined as the resonance wavelength shift per unit change in the RI, the minimum of each transmission spectrum (SPR wavelength) was saved. **Figure 9-c** shows the variation in the resonance wavelength as a function of the variation in the RI, in which the total redshift from 600.00 to 719.00 nm was 119.00 nm. A linear fit was performed, and a coefficient of determination (R^2) of 0.9740 and sensitivity of 2138.95 ± 142.65 nm/RIU were attained.

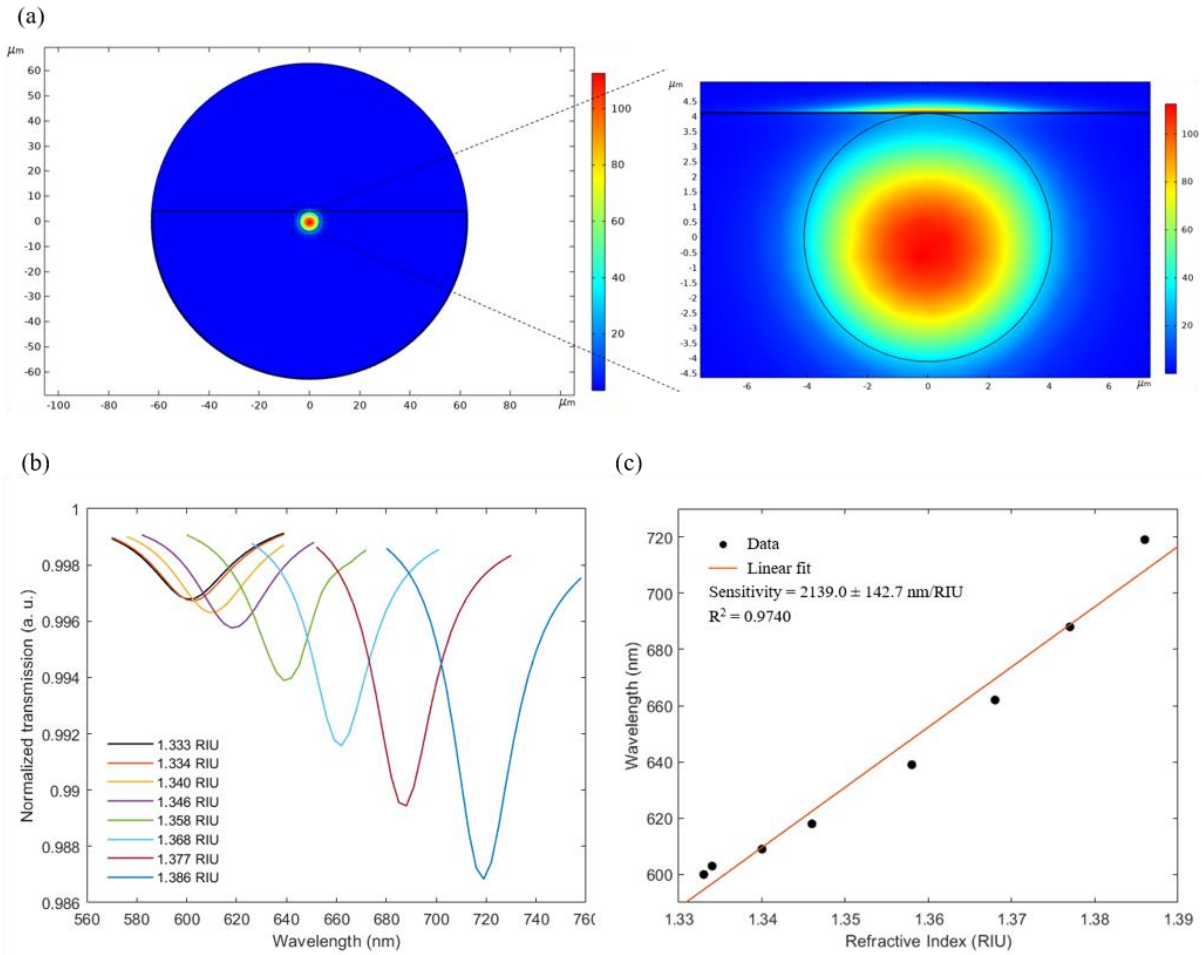

Figure 9 - (a) SPR mode profile; (b) Transmission spectra simulated for glucose solutions with RI ranging from 1.333 to 1.386 in Au-SOF and respective (c) resonance wavelength variation as a function of RI.

IV - Experimental Work

This chapter describes materials, technical equipment information, techniques, and methods used to produce and characterize D-shape SOF and POF biosensors based on SPR for cortisol detection. Firstly, the fabrication of the two types of optical fiber and the respective Au deposition is presented, followed by the characterization of POF and SOF to the RI. The next steps correspond to the biofunctionalization of Au coated on the surface of the sensors, and the experimental test with cortisol, which is described details of how these procedures were performed, following the delineation of the procedures performed in the control test. Furthermore, morphological and chemical characterization by SEM and energy dispersive X-ray analysis (EDX) is described. Afterward, a description of ATR-FTIR characterization of the tested immunosensors is described. Finally, a section on preliminary reuse SOF treatment is outlined.

The last section of this chapter is designed for the presentation and discussion of results.

4.1 Materials and Methods

4.1.1 D-shape SOF Fabrication and Au Deposition

The D-shape SOFs consist of standard single-mode fibers (SMF28) which were acquired from Phoenix Photonics in the United Kingdom, where they were fabricated by side polishing with insertion losses >45 dB (typically 60 dB) and <0.1 dB at RI 1.5 and in air, respectively. These SOFs present a silica core doped with germanium (Ge) and a cladding constituted only with silica. The diameter of the core and the cladding is ~9 and 125 μm, respectively. The RI of the core is ~1.47 and the cladding is ~1.44.

In order to develop a plasmonic D-shape SOF, firstly they were polished, and after, Au was deposited through sputtering technique in Belgium (University of Mons).

To perform the polishing, SOFs were embedded in a V-shaped groove engraved into a quartz block. Afterward, the SOFs were polished until the cladding remained only between 1 and 2 μm. The attained length of the polished region is 10 mm with a tolerance <1 mm, in which 8 mm corresponds to the sensing region, and the remaining 2 mm is taper.

Regarding sputtering, the Au was deposited on one side of the fiber by a sputter-coater (Leica EM SCD 500) under vacuum and argon. The sputtering machine, shown in **Figure 10-a, b,** had incorporated a quartz microbalance that measured the Au thickness. The obtained thickness was 50 nm. **Figure 10-c** shows an Au-SOF.

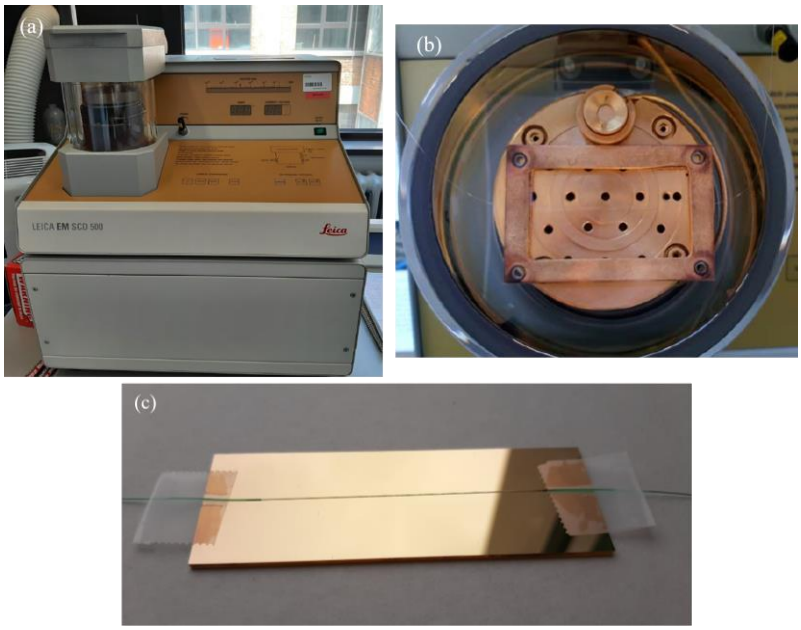

Figure 10 - (a) Sputtering chamber (Leica EM SCD 500), and (b) fiber holder; (c) D-shape Au-SOF.

4.1.2 D-shape POF Fabrication and Au Deposition

D-shape POFs were acquired from an Italian partner (University of Campania Luigi Vanvitelli), where they were fabricated, and the Au deposition was performed. These POFs consist of a PMMA core and a fluorinated polymer cladding, in which the diameter of the core is 980 µm with a cladding thickness of 20 µm, resulting in fiber diameter of 1000 µm. The RI of the core and cladding is 1.49 and 1.41, respectively.

The development of a plasmonic D-shape POF was accomplished in three steps: removal of the cladding and part of the core (along half circumference) in order to perform a D-shape region with 10 mm in length; buffer layer deposition on POF core; and deposition of Au by sputtering technique.

To perform the first step, POF was placed in a resin block to facilitate the cladding and part of the core removal. Therefore, in the first step, the removal was performed by a polishing process. For that, it was used a 5 µm polishing paper to expose the core through 20 complete strokes with a "Figure 8" pattern. Afterward, it was performed the same process using a 1 µm polishing paper [91].

In the second step, the buffer used was Microposit S1813 photoresist with a RI of 1.61 and was deposited by spin coating (6000 rpm for 60 s) on the D-shape region of the fiber, obtaining a thickness of 1.5 µm. The purpose of using this buffer layer was to enhance the Au film adherence and performance since the SPR phenomenon was improved when light propagated inside the fiber and interacted with Au film [48], [92].

Lastly, the sputtering technique was realized by a sputtering machine Bal-Tec SCD 500. The Au film with 60 nm was sputtered through a three-step process, which in each step an Au thickness of 20 nm was deposited after 35 seconds underwent a current of 60 mA [48], [93].

4.1.3 Optical Characterization

After the plasmonic D-shape POF and SOF fabrication, the fibers were characterized to the RI and their sensitivities were later calculated and analyzed. Therefore, POF and SOF were immersed in glucose (D-(+)-glucose (≥99.5), from Sigma-Aldrich) solutions with different known RIs, which allowed us to see the changes in the spectral response for each solution. For that purpose, eight glucose concentrations were prepared with 0, 1, 5, 10, 20, 30, 40, 50 % (w/v). To determine the RI of those solutions, it was used a refractometer (Abbemat 200, Anton Paar) at 21 °C, obtaining RI values of 1.333, 1.334, 1.340, 1.346, 1.358, 1.368, 1.377, 1.386 RIU.

Shortly, the biosensors were first cleaned with deionized (DI) water (from Milli-Q water purification system) and, then, optical measurements were realized for the different glucose concentrations. Before spectra acquisition, the sensor was immersed for 2 minutes in each concentration. Through the transmission spectra, it was possible to analyze the redshift of the SPR signature through the wavelength corresponding to the minimum of the spectra. Lastly, the wavelength variations were graphically represented as a function of the RI of the different solutions. The sensitivity of the sensor was obtained through the slope of the adjustment line:

$$S_n = \frac{\Delta\lambda_{res}}{\Delta n} \tag{20}$$

where $\Delta\lambda_{res}$ corresponds to the variation in the resonance wavelength and Δn the variation in the refractive index.

The experimental setups for both Au-SOF and Au-POF sensors are shown in **Figure 11** and **Figure 12**, respectively. The Au-SOF sensors were placed in a small container constituted of polytetrafluoroethylene (PTFE) with dimensions of 32 × 5 × 3 mm^3 and a volume capacity of 400 µL. As for Au-POF biosensors, due to the resin block in which they are fabricated, was not used a container. The method used to characterize the sensor was by droplet with ~100 µL. The Au-SOF and Au-POF sensors were connected to a light source (tungsten lamp, LS-W7 (7W), manufactured by Sarspec, Portugal), with an emission range from 380 nm to 3000 nm, and a spectrometer which, in turn, was connected to a laptop. The optical transmission spectra were acquired using a spectrometer (FLAME-T-UV-vis manufactured by Ocean Optics, USA) with a detection range of 180-890 nm and resolution of 0.19 nm and displayed on the laptop using OceanView software provided by Ocean Optics. In this software, was applied an integration time at 120 ms, an averaging of scans at 10. Therefore, data was saved and recorded in the wavelength range of 200-890 nm. As data processing, it was necessary to normalize the spectra to the reference spectra obtained with fibers exposed to air and applied two filters (moving average filter, and smooth filter with a span of 0.1 in case of Au-SOF and 0.061 in Au-POF) to reduce noise, using MATLAB software. All experiments were conducted at a temperature of ~21 ºC.

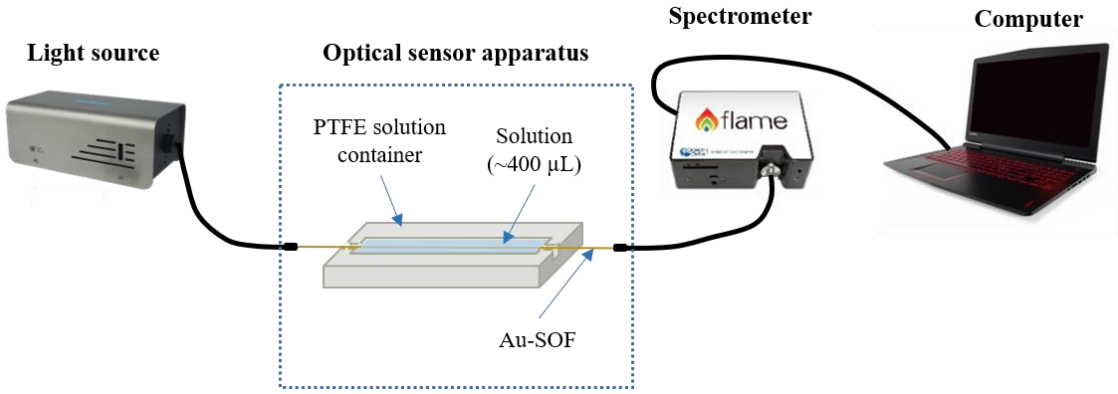

Figure 11 - Schematic representation of the experimental setup for an Au-SOF.

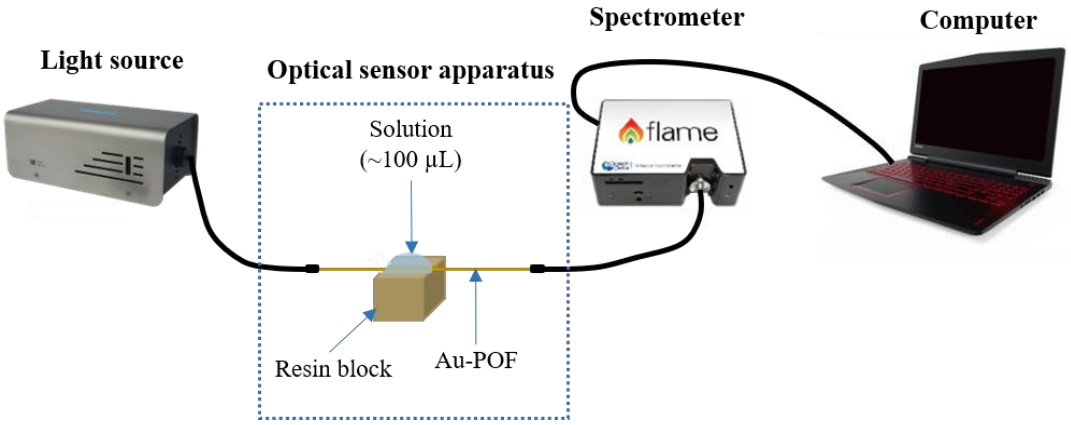

Figure 12 - Schematic representation of the experimental setup used to characterize an Au-POF sensor by droplet.

4.1.4 Functionalization

After the plasmonic D-shape POF and SOF fabrication, four POFs and four SOFs were functionalized with anti-cortisol ABs using the same process on all fibers. All the functionalization steps were monitored and optical spectra were recorded between each step.

The Au surface can be functionalized with ABs through non-covalent bonds, such as electrostatic and/or hydrophobic interactions, by dative bonds between the Au conduction electrons and the sulfur atoms of the AB amino acids, and by covalent bonds. The physicochemical interaction of Au and sulfur is well known to be very strong and, therefore, many approaches take advantage of the chemisorption using thiol derivatives, like the use of cysteamine. Then, the ABs are covalently bonded to the amine-terminated thiol, which is the case of cysteamine, through (*N*-(3- dimethylaminopropyl)-*N*'-ethylcarbodiimide hydrochlorine (EDC) / *N*-hydroxysuccinimide (NHS) chemistry. In **Figure 13** is schematized the biofunctionalization process performed on Au-SOF and Au-POF sensors.

In more detail, the sensors were first cleaned with an aqueous solution of ethanol (10 %) and, then, with DI water and phosphate-buffered saline (PBS, pH = 7.4, 10 mM, from Fisher Bioreagent). The following step was immersing overnight POFs and SOFs in, respectively, 200 µL and 400 µL of an aqueous solution of cysteamine (20 mM) prepared from cysteamine

hydrochloride (≥98 %, purchased from Sigma-Aldrich) to create amine groups on fibers surface. In order to remove the unbounded cysteamine, fibers were washed three times with DI water, followed by a PBS solution. Afterward, the Au-coated fibers were functionalized with anti-cortisol ABs. For that, D-shape POFs were immersed for 2 h in a mixture of 100 µL of anti-cortisol AB (500 µg/mL, acquired from antibodies-online GmbH), 50 µL of EDC (0.2 M, from Merck), and 50 µL of NHS (0.5 M, 98 %, from Merck). Whereas D-shape SOFs were immersed for 2 h in a mixture of 200 µL of AB (500 µg/mL), 100 µL of EDC (0.2 M), and 100 µL of NHS (0.5 M). The EDC and NHS solutions were prepared in PBS. Then, the wash step was repeated, but only in PBS, and the surface of the fibers was passivated with a solution of BSA (100 µg/mL, obtained from Alfa Aesar) for 2 h, using 200 µL in POFs and 400 µL in SOFs. BSA is used to fill the sites that were not covered with AB to not allow non-specific bindings. Lastly, the washing process took place 3 times with PBS.

The experimental setup used for Au-SOF sensors was the same as that used to characterize the sensors, shown in section 4.1.3 (**Figure 11**). For the case of Au-POF sensors, a circular container with a diameter of 8.5 mm and height of 55.5 mm was fabricated by 3D printing that fits the aforementioned resin block, in order to allow the contact of the sensing region to a greater quantity of solution and to ensure that there were no losses. This container of PTFE has a capacity of 400 µL, however, it was only necessary to use 200 µL. Therefore, the experimental setup used for Au-POF sensors is present in **Figure 14**. In the OceanView software, was applied an integration time at 240 ms, an averaging of scans at 10, and a Boxcar Width filter of 10. Subsequently, data was saved and recorded in the wavelength range of 200-890 nm. The data processing was performed in MATLAB software and was necessary to normalize the spectra to the reference spectra (air as the surrounding medium) and apply a smooth filter with a span of 0.1 and 0.061 in Au-SOF and Au-POF spectra, respectively since a moving average filter was applied in the OceanView software. All experiments were conducted at a temperature of ~21 ºC.

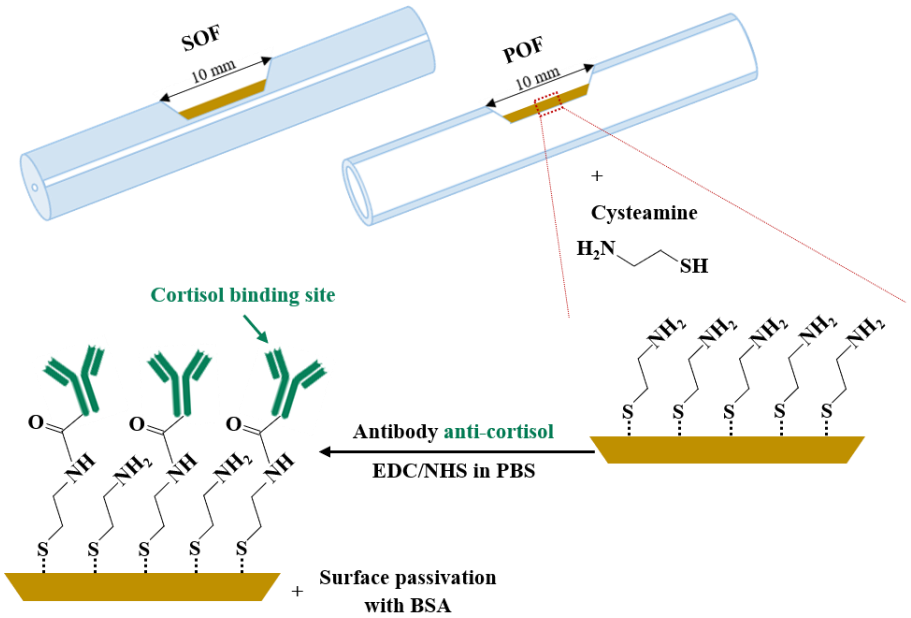

Figure 13 - Optical fiber functionalization steps.

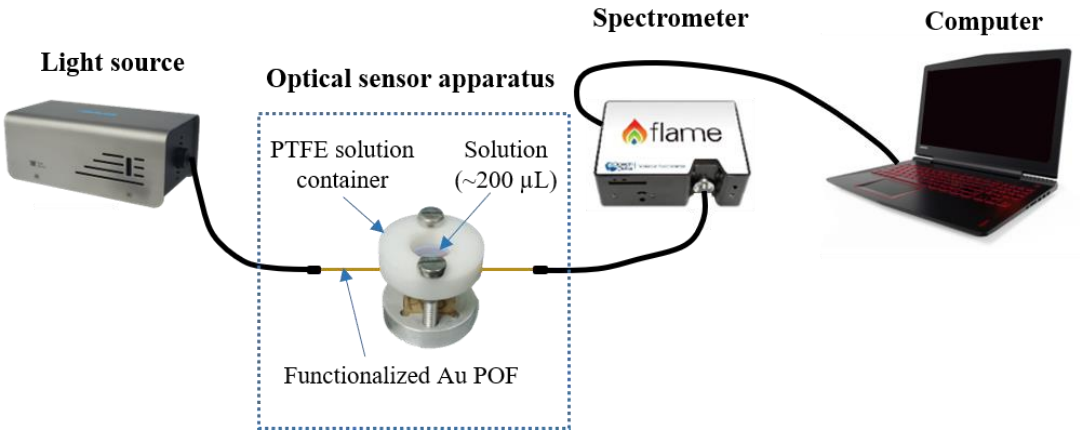

Figure 14 - Schematic representation of the experimental setup for an Au-POF.

4.1.5 Cortisol Detection

After the functionalization process, immunosensors were tested using different cortisol concentrations. to evaluate their performance as immunosensors for cortisol detection.

Cortisol was purchased from Sigma-Merck and was used to prepare 5 solutions in PBS with concentrations ranging from 0.01 to 100 ng/mL from a stock solution of cortisol. Therefore, 1 mg of cortisol was first dissolved in 100 µL of ethanol, to allow solubilization of cortisol in PBS, and then PBS was added to obtain a 1 mg/10 mL stock solution containing 0.1 % ethanol. Subsequently, this solution was diluted until a 1000 ng/mL solution was obtained. From this solution, the remaining concentrations were prepared. In this way, Au-SOF and Au-POF immunosensors were tested for 0.01, 0.1, 1, 10, and 100 ng/mL concentrations. These are concentrations of biological interest, since, in the future, it is aimed to use these immunosensors to detect cortisol in saliva and sweat as well as in water fish tanks for aquaculture.

In the detection tests, to guarantee the formation of the AB-antigen complex, the two types of immunosensors were immersed in each cortisol solution (400 µL for SOF and 200 µL for POF) in ascending order for 20 minutes. After each cortisol solution, the fibers were washed three times with PBS and the transmission optical spectra were acquired while the fibers were still immersed in PBS.

It was decided to keep each concentration of cortisol in contact with the immunosensors for only 20 minutes since from a study previously carried out at the University of Aveiro it was possible to conclude that from 20 minutes onwards the position of the resonance wavelength was substantially stable [7]. Thus, 20 minutes was considered enough time to reach the equilibrium of the cortisol - AB reaction.

The experimental setup used for Au-SOF and Au-POF sensors is shown in **Figure 11** and **Figure 14**, respectively. Data was saved and recorded using the same software and parameters described in section 4.1.4 as well as the data processing. All experiments were conducted at a temperature of ~21 ºC.

4.1.6 Control Test

In order to evaluate the performance of the sensors in terms of selectivity to cortisol, control tests were carried out using a POF and a SOF. Therefore, the fibers were also functionalized with anti-cortisol AB, following the same process as described in section 4.1.4, and tested for four different concentrations: two of glucose and two of cholesterol (≥99 %, purchased from Sigma-Aldrich). For that purpose, prepared concentrations of 50 mg/dL and 500 mg/dL of glucose, and 170 mg/dL and 240 mg/dL of cholesterol were used.

Therefore, the immunosensors were immersed in each solution for 20 minutes (400 µL for SOF and 200 µL for POF), starting with glucose followed by cholesterol. In both cases, the concentrations were tested in ascending order.

To perform these tests, the same experimental setups as shown in **Figure 11** and **Figure 14** for SOF and POF, respectively, were used. Data were equally processed as described in section 4.1.5.

It was decided to use glucose and cholesterol to perform control tests since they are present in the human body, including blood and sweat, like cortisol. Glucose and cholesterol levels vary from person to person and according to the disease if that´s the case. Nonetheless, glucose and total cholesterol levels considered normal for a person without disease should range between approximately 60 to 109 mg/dL and below 200 mg/dL, respectively [94], [95].

4.1.7 SEM and EDX Characterization

SEM is one of the most used techniques for sample characterization since provides information on surface topography and morphology. This analysis uses a focused electron beam to create an enlarged image of the sample. The electron beam scans, in a regular pattern, the sample surface, and the signals resulting from the interaction between the electron beam and the sample are captured to generate the image [96]. These signals can comprise secondary electrons, backscattered electrons, X-rays, among others. The secondary electrons are weakly bonded electrons that are ejected by inelastic scattering, backscattered electrons correspond to primary electrons that reverse their initial direction after scattering events with core level electrons, and X-rays are created when the energy of the incident beam exceeds the electron binding energy [97]. To produce the image, it is necessary that the chamber is in vacuum and the sample is composed with a conductive surface to ensure image quality and minimize the sample charge buildup caused by the electron beam [96], [97].

EDX allows the identification of elements on the sample surface and estimates the elemental proportion at different positions (distribution), providing a chemical mapping of a sample's small area. This technique is applied in conjunction with SEM, and in this analysis, X-rays are emitted from the material due to the interaction of an electron beam with the conducting samples' surface [98]. In more detail, when an electron beam strikes an atom, the atom gets excited leading to the transition of inner shell electrons to higher energy levels. Afterward, an electron from a higher energy level transits to a lower energy level to fill the hole formed due to the atom excitation, resulting in characteristic X-ray emission. The energy of the emitted X-ray corresponds to the difference between the levels from and to which the electron transited. Depending on the series from which the electrons transit, the transitions have different designations, such as K, L, M, N, etc [99], [100]. By moving the electron beam across the sample, several energy peaks are recorded, in

which each characteristic X-ray is recorded at a specific position. Through this procedure is possible to identify different elements [99]. EDX can easily identify elements like silver, gold, palladium, among others. However, elements with low atomic numbers (less than 4) are difficult to detect since they are more difficult to ionize [98], [101].

In the present work, the SEM images were acquired using the TESCAN Vega3 SB equipment available at the Physics Department of the University of Aveiro, in secondary electron mode with a high voltage of 15.0 kV. To perform this procedure, the optical fibers were attached to an aluminum sample holder using double-sided carbon tape. EDX was performed using a Bruker Xflash 410 M Silicon Drift Detector incorporated into the TESCAN Vega3 SB SEM equipment.

4.1.8 ATR-FTIR Characterization

Fourier transform infrared (FTIR) spectroscopy is used to determine the functional groups of a sample and can be applied to identify organic, inorganic, and polymeric materials [98], [102]. In this technique, an infrared radiation beam focuses on an interferometer and a spectral encoding occurs. This means that beams are recombined with different path lengths creating constructive and destructive interferences designated interferogram. Afterward, the beam strikes the sample and some specific frequencies of energy are absorbed, which are unique characteristics of the sample. Then, for all frequencies simultaneously, the interferogram signal is measured by the detector in energy versus time. The desirable spectrum is obtained when the interferogram automatically subtracts the background spectrum from the sample spectrum by Fourier transformation computer software [102].

Summarily, samples are stricken with infrared radiation, and some radiation is absorbed, which is converted to vibrational or rotational energy. A spectrum is attained at the detector and usually ranges from 4000 to 500 cm^{-1}. This spectrum is considered the molecular fingerprint of the studied sample [98].

Usually, an FTIR spectrum is divided into four regions owing to the bond types. In the region of higher wavenumber ranging from 2500 to 4000 cm^{-1} are present the single bonds, such as O-H, C-H e N-H. From 2000 to 2500 cm^{-1} is detectable the triple bond, and the double bond appears from 1500 to 2000 cm^{-1}. The remaining region belongs to a complex pattern of vibrations, characteristic of the molecule as a whole [102].

In this work an ATR-FTIR technique was used, in which the spectra acquisition was performed in an infrared spectrometer (Bruker Alpha Platinum, Germany) equipped with an attenuated total reflectance (ATR) accessory, with a resolution of 4 cm^{-1} and 32 scans, in the mid-infrared region (4000-500 cm^{-1}). This spectroscopic technique was only performed in two D-shaped SOFs, after the biofunctionalization and cortisol detection procedures. It was inapplicable to perform this technique in a D-shaped POF due to the presence of the resin block. These analyses were performed in a room with a controlled temperature and humidity of 25 °C and 35 %, respectively. Further, it was only executed after the experimental tests with cortisol since the fiber is broken by the crystal in the sensing region when using this technique.

In ATR-FTIR spectroscopy, a crystal is used to trigger the phenomenon of TIR and, consequently, the creation of an EW [103]. When the EW is generated, the intensity of the reflected light is reduced leading to a phenomenon called ATR. When the sample is in contact with the crystal, the EW is absorbed by the sample. Using the ATR technique together with infrared

spectroscopy allows samples to be examined directly in a solid or liquid state without additional preparation and is a quick method [104].

4.2 Results and Discussion

4.2.1 Optical Characterization

To evaluate the performance of the sensors to the changes in RI, they were submitted to glucose solutions with different concentration values. Therefore, is possible to observe in **Figure 15-a** and **Figure 15-b** the spectral wavelengths responses owing to the variation of the RI, for Au-SOF and Au-POF sensors, respectively. As can be seen for both sensors, with increasing glucose concentration, a shift to longer wavelengths is noticeable. Hence, the wavelength shifts were used to evaluate the sensitivity of the proposed sensors. The sensor sensitivity is defined as the resonance wavelength shift per unit change in the RI. The SOF resonance wavelength changed from 614.31 nm to 704.05 nm which corresponds to a total redshift of 89.74 nm. The POF coated with Au presented a total redshift of 79.90 nm from 599.30 nm to 679.20 nm.

As already mentioned in section 4.1.3, the sensor's sensitivity is obtained by determining the slope of the fit calibration curves of wavelength as a function of RI, since the shift of the transmission spectrum peaks is correlated to the increasing of glucose concentration and, consequently, to RI increase. Thus, a linear fit was performed in both cases, attaining a higher coefficient of determination and sensitivity in SOF than in POF. As represented in **Figure 16**, SOF presented an R^2 of 0.9817 and a sensitivity of 1646.67 ± 91.66 nm/RIU, whereas POF exhibited an R^2 of 0.9776 and a sensitivity of 1566.81 ± 96.87 nm/RIU.

Regarding SOF, through simulation (section 3.1) it was obtained a sensitivity of 2138.95 ± 142.65 nm/RIU, which is higher than the experimental sensitivity (1646.67 ± 91.66 nm/RIU). In the same way, the total redshift also presented a higher value (119.00 nm comparing with 89.74 nm). The observed differences may be related to the fact that at the time of simulation, the parameters used for the fiber may not have been the same as the real parameters, there may be slight differences in core radius, RIs, and Au layer thickness, which may imply a difference between the calculated modes and the real modes. In addition, was considered a cladding thickness of 0 µm between the cut and the core, while, experimentally SOF presented a cladding thickness of 1 to 2 µm, leading to a decrease in the experimental sensitivity compared to the simulated one since the light does not directly interact with the Au layer. Furthermore, the lower sensitivity obtained experimentally may be related to the fact that the Au layer cannot be all homogeneous along the entire surface of the D-shape region. Another issue, experimentally, the light passes through the fiber and when enters the D-shape zone presents an adjustment distance to the new geometry, in which there may be some light losses in this region without being related to losses in the Au layer. This effect was not simulated and may have changed the results.

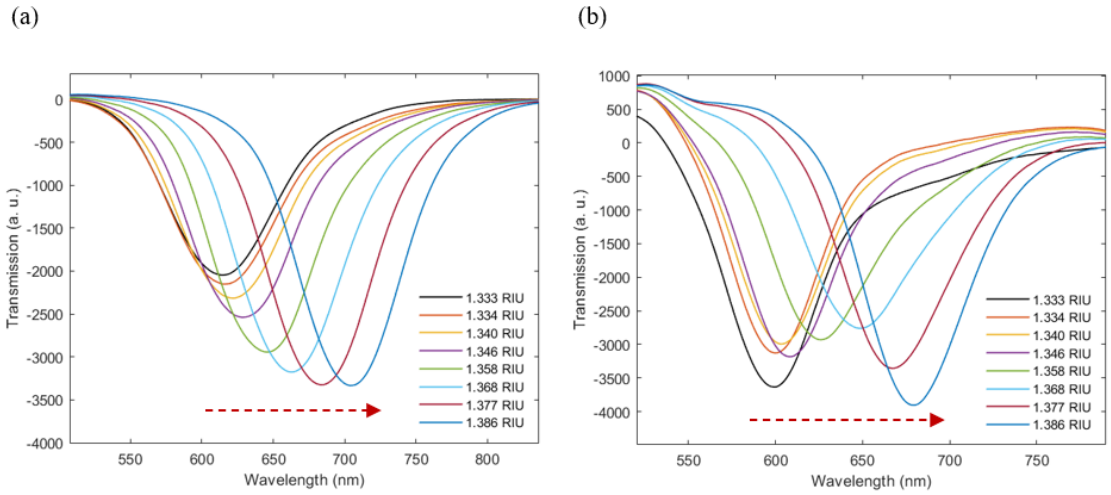

Figure 15 - Transmission spectra recorded for glucose solutions in a concentration range from 0 to 50 % in (a) Au-SOF and (b) Au-POF.

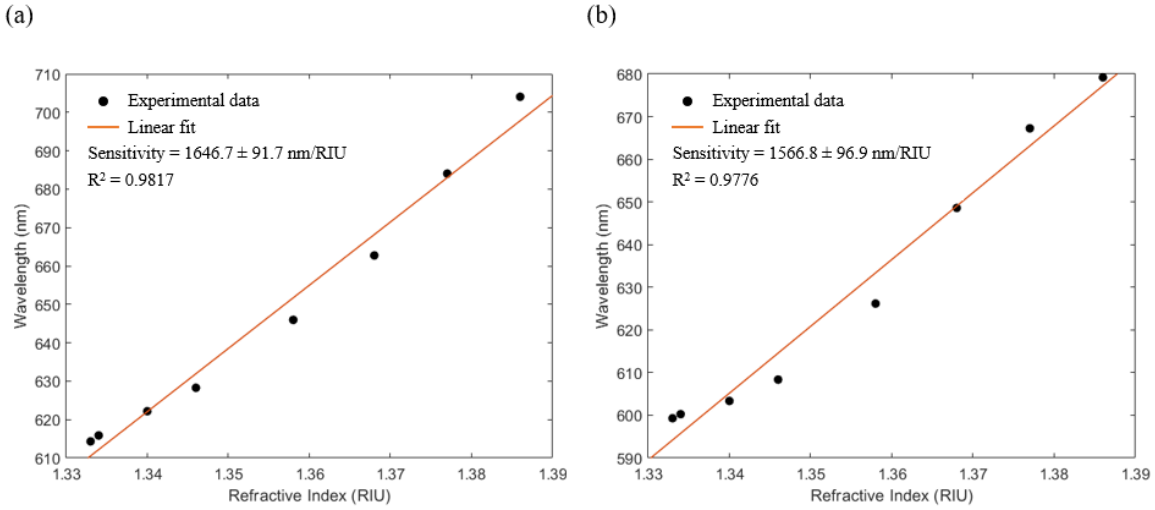

Figure 16 - Resonance wavelength variation as a function of RI for (a) Au-SOF and (b) Au-POF, showing the linear fittings.

4.2.2 Functionalization

After performing the characterization of the sensors to the RI, it was performed an important step for the production of optical fiber immunosensors for cortisol detection, the functionalization procedure. This procedure aimed to ensure the binding of anti-cortisol AB to the Au-SOF and Au-POF surfaces and passivate the remaining surface to reduce non-specific interactions, promoting only cortisol immobilization through the AB-antigen complexation reaction.

All the steps performed during the modification process of Au-SOF and Au-POF were analyzed through the acquisition of transmission spectra as shown in **Figure 17**. Besides, a spectrum in PBS was recorded, and all the transmission spectra were acquired after washing the fibers in PBS. Regarding the first step, the fibers were immersed in cysteamine solution overnight to allow a self-organized monolayer formation on the fibers' surface. This process led to a redshift of the SPR

signature of 9.11 ± 5.90 nm in Au-SOF and 9.83 ± 6.84 nm in Au-POF, due to the variation of the surrounding RI. The immobilization of anti-cortisol AB was confirmed with the presence of a large redshift of 19.07 ± 11.42 nm in Au-SOF and 16.72 ± 8.81 nm in Au-POF after this biofunctionalization step, which can be seen through the displacement of the transmission spectra. The total redshift caused by the biofunctionalization procedure was 19.69 ± 11.52 nm in Au-SOF and 16.67 ± 9.02 nm in Au-POF. This means that the passivation surface with BSA caused only a redshift of 0.62 nm in the case of Au-SOF and practically none regarding Au-POF. All the wavelength shifts occurred due to an increase of the RI of the surface of the Au-coated fibers. **Figure 18** shows the average redshift of four assays caused by every step of the biofunctionalization procedure in the case of Au-SOF and Au-POF. The high error bar present in the SOF graph may be related to the polishing depth applied to the fibers. In more detail, the polishing depth can be slightly different between sensors causing them to have vaguely different responses. The variation in results between essays using POF can be associated with the difference in D-shape length observed in various POFs as explained below in section 4.2.3.

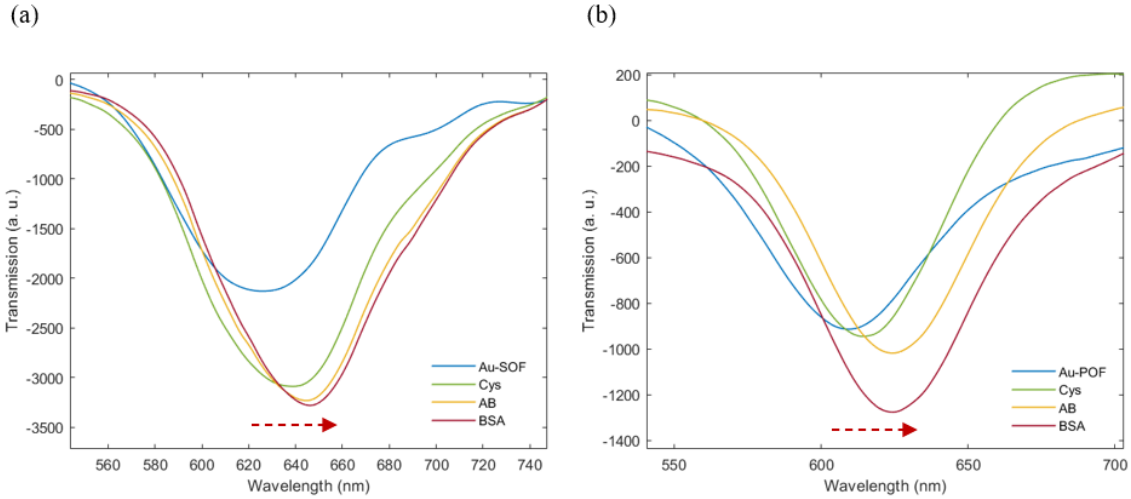

Figure 17 - Spectra attained after each functionalization step of (a) Au-SOF and (b) Au-POF.

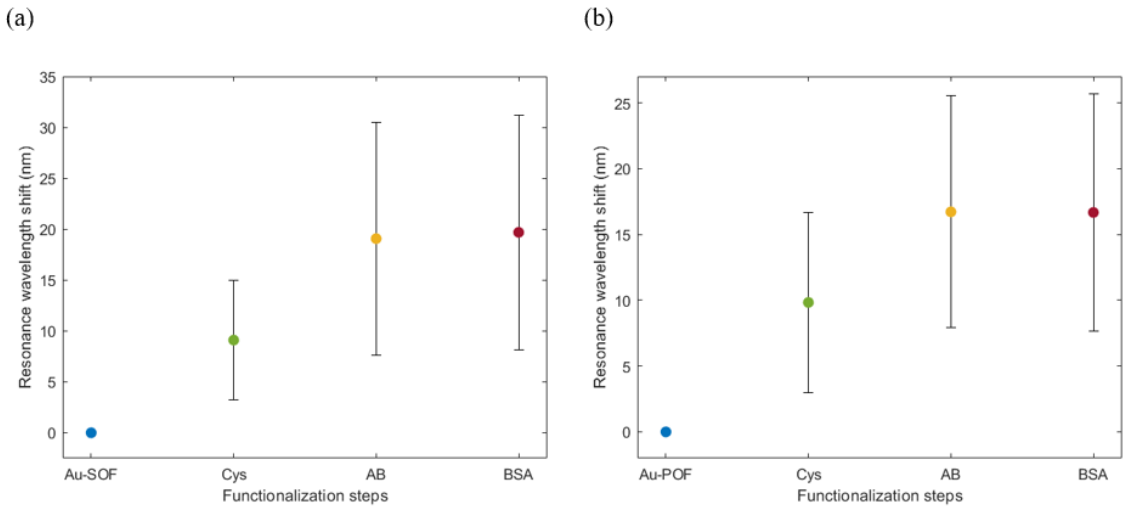

Figure 18 - Resonance wavelength shifts obtained in PBS buffer solution after each biofunctionalization step (results for quadruplicates are presented) for (a) SOFs and (b) POFs coated with Au.

4.2.3 Cortisol Detection

After the biofunctionalization procedure, Au-SOF and Au-POF immunosensors were tested for different cortisol concentrations and the respective transmission spectra were acquired as shown in **Figure 19**. These optical spectra were obtained after washing the sensors with PBS and immersed in the same buffer solution.

Figure 19-a, b shows the results for the best essay of Au-SOF and Au-POF, respectively, where is possible to observe a redshift to longer SPR wavelengths. The shift is more notable in Au-SOF than Au-POF, nonetheless, it is present in both situations. To analyze the responses of the 4 essays in each case, the wavelength shift was calculated by subtracting the SPR wavelength at 0 ng/mL from the SPR wavelength at a given cortisol concentration for each essay, being the SPR wavelengths the minimum of the transmission spectra. Then, the average of the SPR wavelengths was taken. As mentioned in the 4.1.5 section, the spectra were smoothed applying a smooth filter in MATLAB and the minimum value was also attained using an appropriate MATLAB function.

The Au-SOF presented a logarithmic response to the cortisol concentration ranging from 0.01 to 100 ng/mL with an R^2 value of 0.9975 as shown in **Figure 20-a**. Moreover, the total redshift was 3.70 ± 0.39 nm and the attained logarithmic sensitivity (LS) (shift of the SPR wavelength per unit change in the logarithm cortisol concentration) was 0.65 ± 0.02 nm/log(ng/mL). The standard deviation in resonance wavelength was calculated for each concentration since the experiments were performed on 4 different sensors. From **Figure 20-a**, it can be seen that for concentrations ranging from 0.01 to 1 ng/mL, the reproducibility of the immunosensor was poor. Only from 10 ng/mL can it be considered a favorable reproducibility. The observed poor reproducibility for lower concentrations can be related to the differences in polishing depth between SOFs, leading to slightly different responses as explained in section 4.2.2.

Thus, as sweat cortisol levels range from 8.16 to 141.70 ng/mL and cortisol concentrations in water with high fish density is ~3.08 ng/mL, this means that these immunosensors are more suitable for application in human health through the detection of cortisol in sweat than for application in aquaculture.

In contrast, the Au-POF immunosensor did not present a logarithmic response as can be seen from R^2 which has a value of 0.5589. **Figure 20-b** shows that there is no ever-increasing shift with increasing cortisol concentration from 0.01 to 100 ng/mL, therefore, this immunosensor did not respond to cortisol. The standard deviation in resonance wavelength was calculated for each concentration since the experiments were performed on 4 different sensors and, as can be seen, no response was obtained since the reproducibility of the immunosensor was poor. Thus, it is not possible to obtain a cortisol detection response when applying the average of the responses from the 4 essays. One of the reasons for no reproducibility may be related to the fact that the D-shape zone is not very controlled at the time of manufacture. Through **Figure 21**, it can be seen that for different fibers the D-shape zone has different lengths. When the D-shape zone is larger, not all of that zone is in contact with the solutions, having differences in the RI along the D-shape region. Therefore, when light passes through the fiber there will be light losses throughout the entire D-shape zone, in which not all of that light interacts with the solutions, leading to changes in SPR wavelength and, consequently, in sensors responses.

Figure 22 shows the response of a POF immunosensor with a D-shape zone of exactly 10 mm, in which it is possible to observe an increase in wavelength shift with increasing cortisol concentration from 0.01 to 100 ng/mL, having no blueshifts and a total redshift of 2.10 nm. The

obtained LS was 0.50 ± 0.02 nm/log(ng/mL) with an R^2 of 0.9941. Therefore, it is necessary to perform tests with POFs that have the same D-shape zone length in order to verify whether there is reproducibility using POF immunosensors.

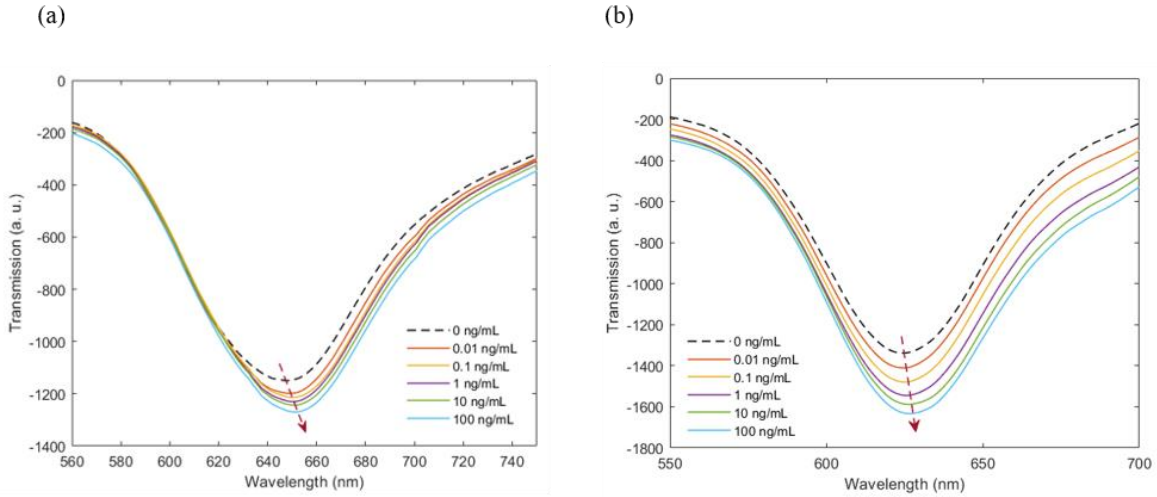

Figure 19 - Spectral responses of the functionalized (a) Au-SOF and (b) Au-POF immunosensors, acquired in PBS, as a response for cortisol solutions in a concentration range from 0.01 to 100 ng/mL, after incubation during 20 min.

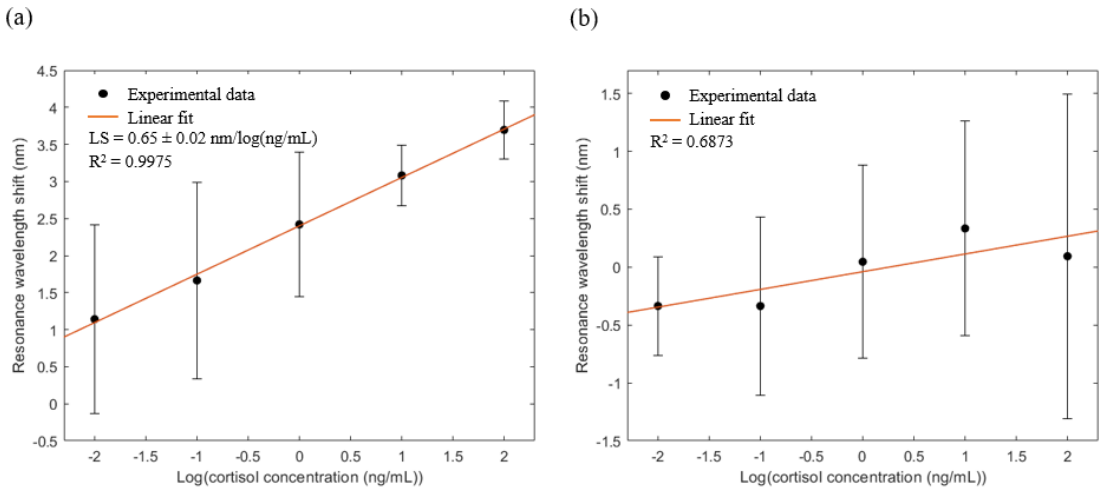

Figure 20 - SPR signature wavelength shift as a function of the logarithm of cortisol concentration (linear fitting for an average of 4 tested sensors) for (a) Au-SOF immunosensors and (b). Au-POF immunosensors.

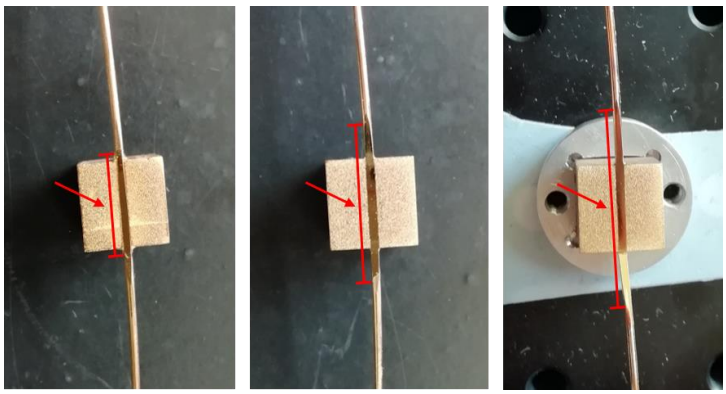

Figure 21 - Examples of Au-POFs with different D-shape lengths.

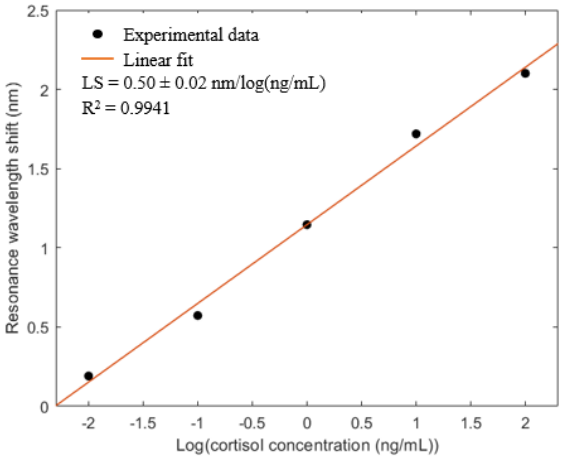

Figure 22 - SPR signature wavelength shift as a function of the logarithm of cortisol concentration for one Au-POF immunosensor.

4.2.4 Control Test

To evaluate the selectivity of the immunosensors, a control test was performed in Au-SOF and Au-POF immunosensors although with POF no favorable results were obtained in cortisol detection.

As aforementioned in section 4.1.6, the fibers were equally functionalized with anti-cortisol AB, however, they were tested for different analytes, including glucose and cholesterol, which do not have an affinity with the anti-cortisol AB. **Figure 23** shows the histogram comparison of the resonance wavelength shift as a function of different cortisol, glucose, and cholesterol concentrations in the case of Au-coated SOF and POF immunosensors.

It can be observed through histogram (**Figure 23-a**) that the total resonance wavelength shift was approximately 3.70 nm when using cortisol analyte and the resonance wavelength shift for 50 mg/dL was small compared with most of the cortisol concentrations. The remaining concentrations also presented a small shift, but in these cases, it was negative. This means that in general, the Au-SOF sensor responded to glucose and cholesterol concentrations, with the SPR wavelength shifting to lower values at almost all concentrations except for 50 mg/dL of glucose. The positive response with glucose was probably due to non-specific interactions promoted by physical adsorption of the glucose onto the SOF surface, leading to the conclusion that perhaps surface passivation was not efficient. The negative response probably occurred due to the interaction of BSA with glucose and cholesterol and its removal from the surface, leading to a decrease in the surrounding RI and, consequently, to a shift in the resonance wavelength to lower values.

In this case, LOD was calculated applying a conservative approach [105], given by:

$$LOD = mean_{blank} + 3\sigma_{blank} \quad (21)$$

being blank the control analyte responses and σ_{blank} its standard deviation, which resulted in a LOD of 1.46 ng/mL.

Regarding POF, is possible to observe through **Figure 23-b** that the Au-POF immunosensor did not respond to cholesterol concentrations. Nonetheless, the immunosensor showed a very small response to cortisol analyte compared to glucose since its shift was much lower than the shift promoted by glucose. This means that the POF sensor showed a response to glucose and not to cortisol.

(a)

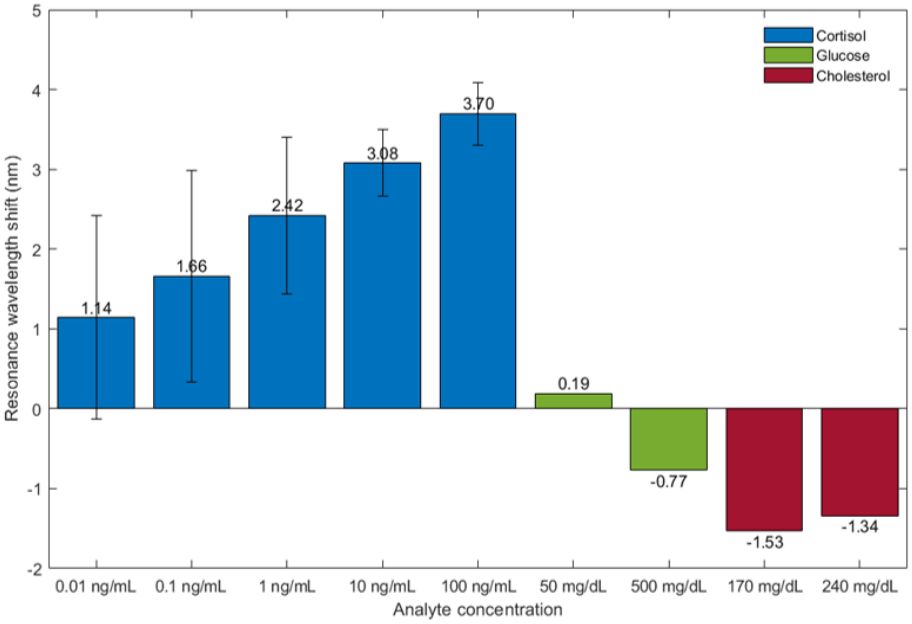

(b)

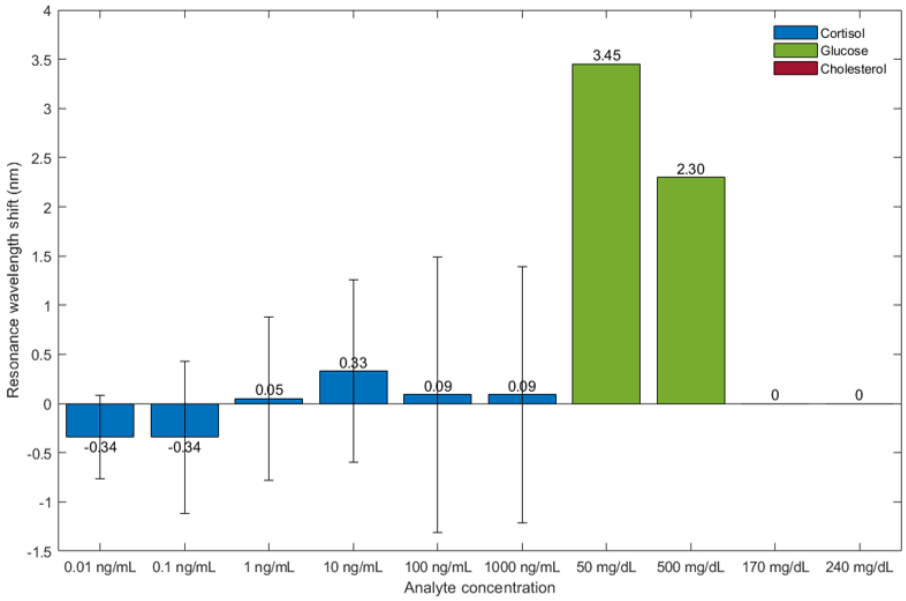

Figure 23 - Histogram comparison of the shift in resonance wavelength between when is used different analytes for the same anti-cortisol AB in (a) Au-SOF immunosensors and (b) Au-POF immunosensors.

4.2.5 SEM and EDX Characterization

In order to assess the surface topography and morphology, as well as the fiber elemental composition, an Au-coated SOF and POF were observed by SEM (**Figure 24-a, h** and **Figure 25-a**, respectively) and EDX.

In the case of SOF, the EDX spectrum in **Figure 24-b** shows clear peaks of oxygen (O), Al, Si, and Au, which correspond to the peaks with higher intensity values. In **Figure 24-c, d, e, f** is possible to visualize the individual Au, Si, Al, and O maps, respectively. The presence of Au, Si, and O is in line with the expected results. As can be seen in **Figure 24- d, e**, Si and O are present in all the fibers' surface since it is composed with silica (SiO_2). Through **Figure 24-c** and SEM image (**Figure 24-a**) is possible to prove that Au is uniformly dispersed throughout the entire surface of the fiber without flaws, which indicates a uniform deposition. As already mentioned in section 4.1.7, the sample holder is made of Al which justifies the peak with high-intensity corresponding to Al in EDX spectrum, and its presence in the surroundings of SOF (**Figure 24-f**).

In the SEM image (**Figure 24-a**) it is also possible to observe laterally the presence of a few crystals which are composed of chlorine (Cl), as shown by the chemical map in **Figure 24-g**. To further analyze these crystals, another SEM image (**Figure 24-h**) and EDX spectrum (**Figure 24-i**) were saved, where it is possible to observe the presence of more protruding crystals. As can be seen from the EDX spectrum and the overlap of all maps in **Figure 24-j**, the crystals are also composed of Na. This points to the presence of sodium chloride (NaCl) crystals. This characterization was carried out after functionalization and the tests with cortisol, in which PBS was used for the last and throughout the tests for cleanings, leading to the formation of NaCl crystals that can be seen by SEM images. Except the crystals, it is possible to observe a clean gold surface with practically no defects even after using the fiber during functionalization and cortisol detection.

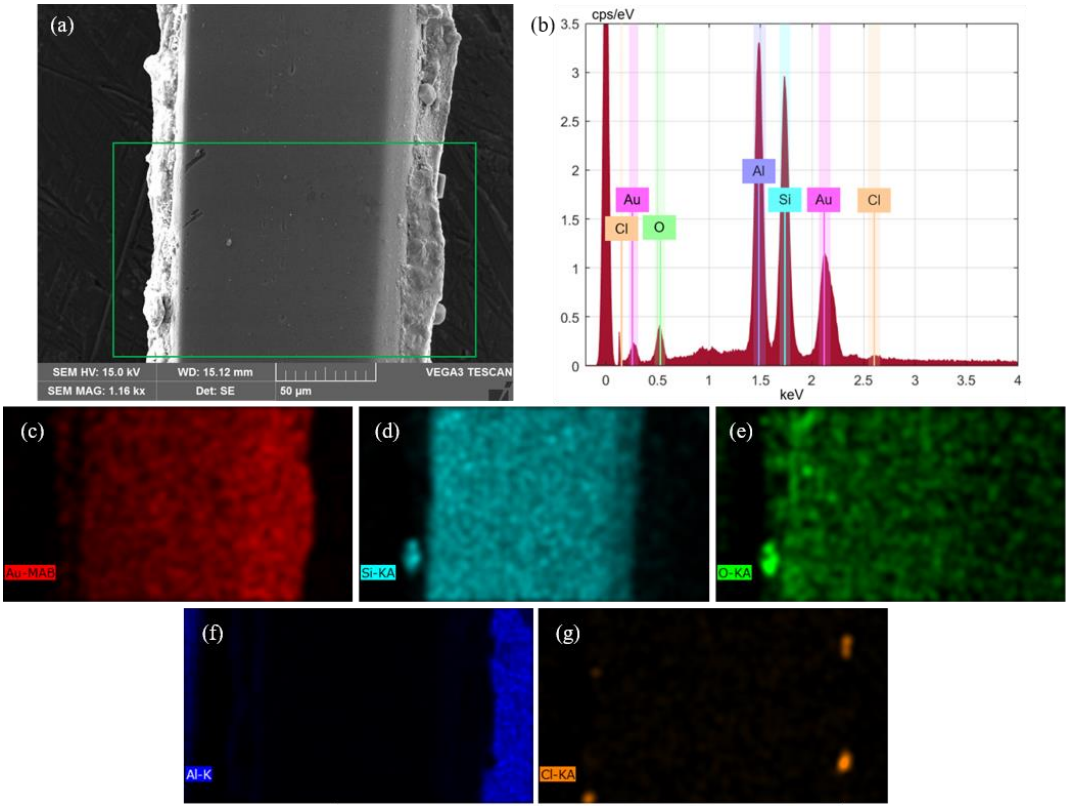

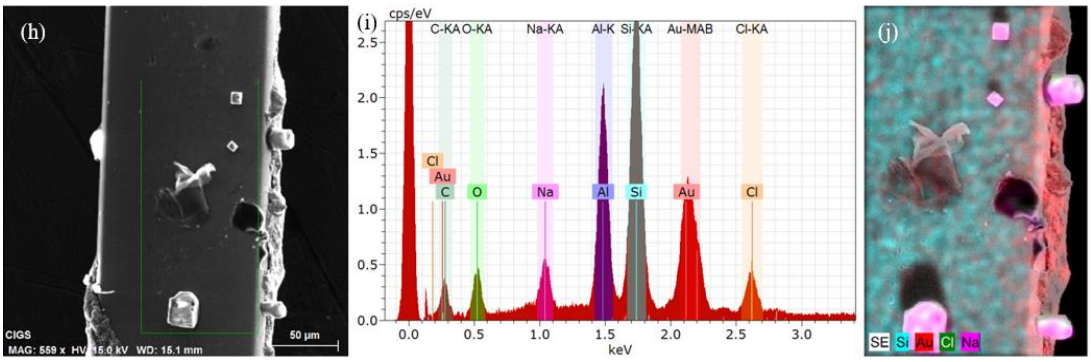

Figure 24 - SEM images, EDX spectra, and chemical maps of an Au-SOF.

In **Figure 25** it is possible to observe an SEM image, the EDX spectrum, and the chemical maps of a POF coated with Au after functionalized and tested for several cortisol concentrations. POF is composed of PMMA ($(C_5O_2H_8)_n$), therefore, the presence of C (**Figure 25-d**) and O (**Figure 25-e**) along the entire surface of the fiber is justified. As with SOF, it is also possible to verify from **Figure 25-c** that the deposition of Au was uniform since the Au is evenly dispersed over the entire surface of the fiber. Through the SEM image (**Figure 25-a**) and the chemical maps in **Figures 25-f, g**, the presence of NaCl crystals can also be observed. The presence of these crystals has the same justification as in the case of SOF since PBS was also used in the procedures of functionalization and detection of cortisol.

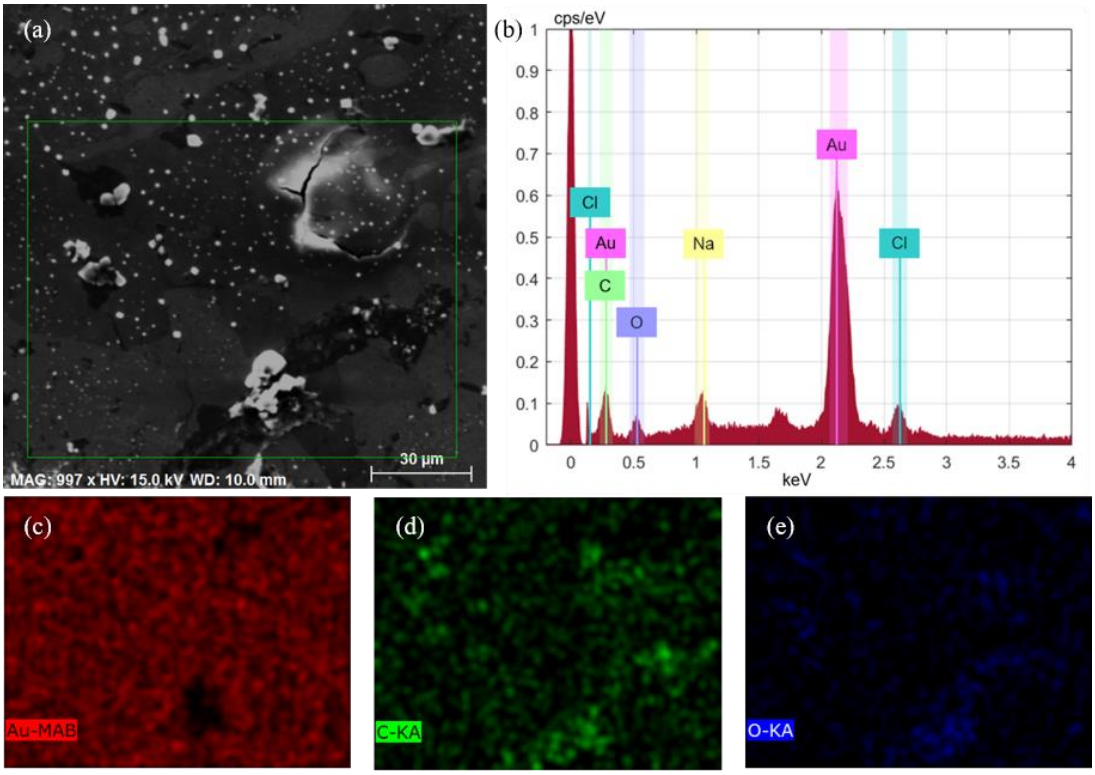

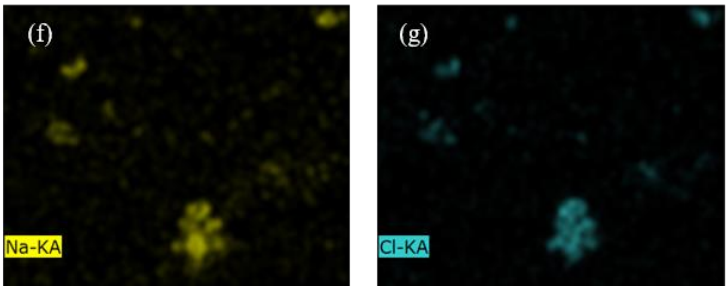

Figure 25 - SEM image, EDX spectrum, and chemical maps of an Au-POF.

4.2.6 ATR-FTIR Characterization

As already described in section 4.1.8, ATR-FTIR analyses are used to discover the functional groups present in a sample, being the spectrum the molecular fingerprint of that sample.

Figure 26 shows the FTIR spectra of the optical fiber references: SOF and Au-SOF. In these spectra is possible to see peaks that correspond to characteristic bonds of the presence of silica, such as Si-O and Si-O-Si at 801 and 1093 cm^{-1}, respectively.

Two Au-SOF immunosensors were analyzed by this technique after the experimental test, including functionalization and cortisol detection, since this approach breaks the fiber in the sensing zone, preventing future use of this fiber.

Thus, in **Figure 27** is possible to observe the FTIR spectrum of Au-coated SOF and two spectra of Au-SOFs immunosensors after functionalization (Au-SOF 1 and Au-SOF 2). After the experimental test using immunosensor 1, this fiber was kept under ambient conditions for 6 months until be analyzed by FTIR. The second immunosensor was analyzed the day after the test. Through the spectrum of Au-SOF 2 is possible to notice amide I, amide II, and amide A, which are characteristic peaks of a protein (AB and BSA). Furthermore, between 1300 and 1500 cm^{-1} is observed other peaks attributed to side chains of the proteins. The presence of these proteins is also confirmed with the apparent shift of the Si-O-Si bond, which occurred due to the contribution of OH groups from the side chains of the proteins. In Au-SOF 1, is present the stretching vibration of C=O, amide A is absent and amide I and amide II are almost unnoticed. This means that the AB and BSA must be denaturated since there was a 6-month time lag between functionalization and FTIR analysis of the fiber. Thus, sensors must be used for detection tests shortly after surface functionalization since the functionalization layer is no longer effective if stored at room temperature, or a specific protocol for storage should be studied in order to extend storage lifespan. Nevertheless, through ATR-FTIR it was possible to verify that the surface of the silica fibers was functionalized owing to the presence of characteristic peaks of AB and BSA.

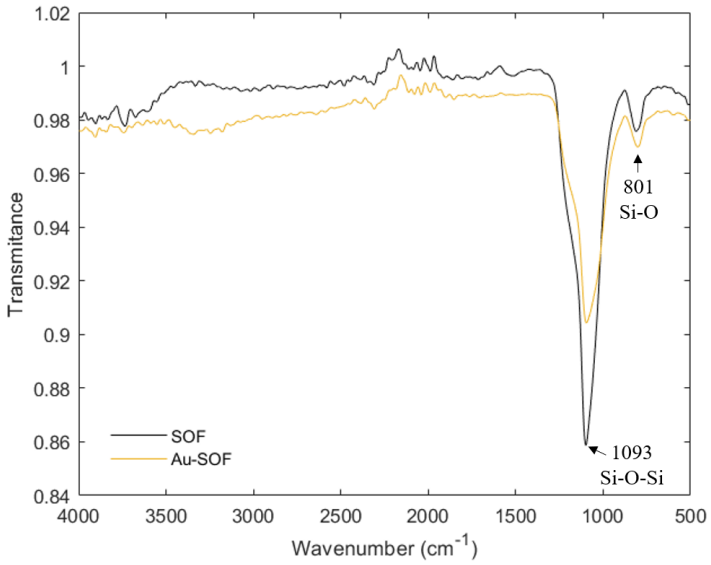

Figure 26 - FTIR spectra of the SOF and Au deposited on a SOF.

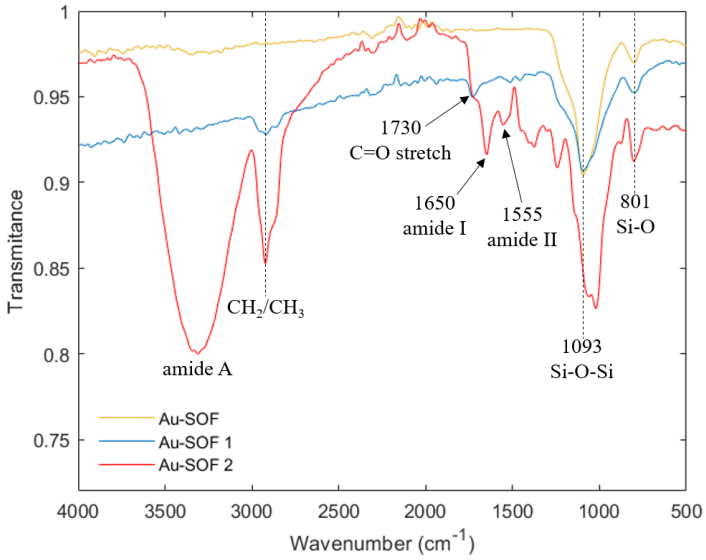

Figure 27 - Comparison of the FTIR spectra of Au-SOF and tested SOFs: (blue) Au-SOF kept in ambient conditions for 6 months until FTIR analysis; (red) Au-SOF analyzed the day after cortisol detection.

4.3 Preliminary Reuse SOF Treatment

After all this process of studying optical fibers for different concentrations of cortisol, with the purpose of successfully reuse optical fibers in the future, a chemical process was performed on the two broken SOFs after the first FTIR to remove all the functionalization layers. This process is an innovation since has never been carried out in optical fiber biosensors. The chemical process consisted of removing the thiol group (from cysteamine) from the Au surface using a solution of NH_4OH – H_2O_2 – H_2O as described in [106]. For that, was used a 2:1:66 volume ratio corresponding to NH_4OH, H_2O_2, and DI H_2O, respectively. Therefore, in a glass cup was formed a

mixture of 65 µL of NH_4OH, 26 µL H_2O_2 and 10 mL of H_2O with a basic pH of ~10.95. Afterward, the SOFs were immersed in 400 µL of the mixture for 30 minutes. In the end, the fibers were washed two times with ethanol and 3 times with DI water. This procedure was carried out at an ambient temperature of 21 ºC and relative humidity of 78 %. The experimental setup used in this chemical process was the same applied in the previous tests with SOFs as shown in **Figure 11**.

In order to verify if the fibers did not contain the proteins resulting from the functionalization after the treatment, the two broken fibers were submitted again to FTIR analysis. As can be seen from **Figure 28**, after treatment, the amide I, amide II, and amide A characteristic peaks of a protein (AB and BSA) disappeared, as well as the peaks attributed to side chains of the proteins between 1300 and 1500 cm^{-1}. Moreover, due to the OH groups from the side chains of the proteins, a shift of the Si-O-Si bond was noticed, however, that shift is no longer present after the treatment.

In conclusion, all characteristic peaks of proteins disappeared, which is indicative of the absence of functionalization layers. The success of this treatment can also be proven by comparing the spectra of treated fibers with the spectrum of a fiber that has never been functionalized and tested. Through this comparison, the similarity of the spectra was verified. Nonetheless, comparing with the spectrum of Au-SOF 2 treated, Au-SOF 1 treated presented a spectrum more similar to the spectrum of the unused fiber (Au-SOF). As aforementioned in section 4.2.6, Au-SOF 1 was stored at room temperature for 6 months, and AB and BSA proteins became denaturated. Therefore, the time between the use of the fiber for testing and its treatment with the chemical process can be an important factor in the successful reuse of optical fibers. In the future, treated fibers will be functionalized and tested for cortisol to validate the reuse method.

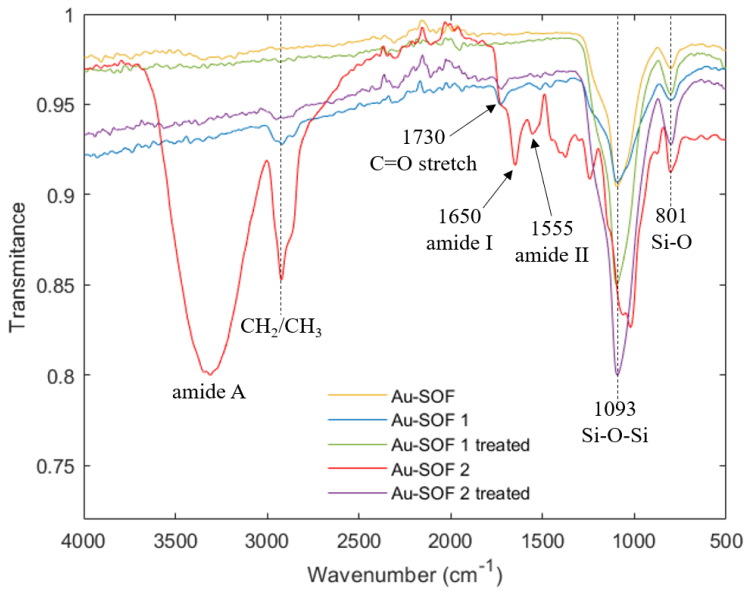

Figure 28 - Comparison of the FTIR spectra of Au-SOF (yellow), tested Au-SOFs (blue and red), and regenerated Au-SOFs (green and purple).

V - Conclusions and Future Outlook

The aim of this dissertation consisted of the development of SPR-based optical fiber immunosensors capable of detecting a stress biomarker, cortisol. The different used immunosensors were composed of SOFs or POFs modified to a D-shape structure and coated with an Au film to allow the triggering of the SPR phenomenon. Initially, the optical characterization of these sensors for different RI values was simulated, in which it was possible to obtain a sensitivity of 2138.95 ± 142.65 nm/RIU with SOF. Experimentally, immunosensors were also optically characterized for different glucose RI values, showing a sensitivity of 1646.67 ± 91.66 nm/RIU (lower than the simulated sensitivity, however, with the same order of magnitude) and 1566.81 ± 96.87 nm/RIU in the case of SOF and POF, respectively.

Subsequently, eight immunosensors (four with SOF and four with POF) were subjected to a functionalization process (cysteamine, AB anti-cortisol, and, finally, BSA), obtaining a total redshift of 19.69 ± 11.52 nm in Au-SOF and 16.67 ± 9.02 in Au-POF, followed by detection assays with cortisol. The Au-SOF immunosensor responded logarithmically to the presence of cortisol and an R^2 of 0.9975 was obtained for the linearized plot. For a tested concentration range from 0.01 to 100 ng/mL, a LS and a LOD of 0.65 ± 0.02 nm/log(ng/mL) and 1.46 ng/mL were attained, respectively. Regarding POF, it did not show a clear response to the presence of cortisol, which presented an R^2 of 0.6873 through linear fit in a logarithmic response. In more detail, the resonance wavelength did not continuously shift to higher values with increasing cortisol concentration and rather distinct responses of immunosensors were observed. SOF immunosensors presented a poor reproducibility for concentrations ranging from 0.01 to 1 ng/mL and POF immunosensors for all concentrations, which can be associated with the variation in polishing depth between SOFs and the difference in D-shape zone length between POFs. The D-shape Au-POF immunosensor did not present the desired tendency with 4 assays and, therefore, it is not a viable solution to proceed with the intended applications, such as integrating into bandages or using in fish production tanks. However, one assay using a POF with exactly 10 mm of D-shape showed good results (total redshift of 2.10 nm and LS of 0.50 ± 0.02 nm/log(ng/mL)). Therefore, it is necessary to perform more tests with POFs that have the same D-shape zone length of exactly 10 mm in order to verify the reproducibility of the POF immunosensor.

From the results of the control tests, it was concluded that the presence of glucose and cholesterol led to a response of both immunosensors, except for cholesterol in POF. It is necessary to perform more control tests of this nature with other relevant interfering compounds. Moreover, measuring mixtures of cortisol and those compounds is also necessary to evaluate if there is a relevant interference to the immunosensors response to cortisol.

In order to reuse optical fibers in the future for biosensors production and, thus, reduce production costs and support sustainability, two used SOFs were subjected to a chemical process to remove the functionalization layers. To check if the chemical process was a success, ATR-FTIR analysis was performed, demonstrating an effective proteins removal from the functionalization layer.

In addition, the perspectives for future work include making progress with D-shape Au-SOF and Au-POF in terms of simulation, and experimentally with D-shape Au-SOF since showed satisfactory results. Moreover, it has other advantages, such as the ease of performing ATR-FTIR tests to study the reuse since with D-shape POF it is not practical due to the presence of the support cube, and it is easy to manufacture, in which a SOF polishing mechanism is currently being

developed at the University of Aveiro to create the D-shape structure. Thus, it is intended to perform more tests to further prove the reproducibility of D-shape SOF immunosensors mainly for lower concentrations, and make a protocol to test these fibers using water samples from fish tanks and samples of sweat, human urine, among others. After all this process, it is intended to develop viable support for application in fish tanks.

In terms of reuse, after the chemical process, it is desirable to perform tests with cortisol to be able to compare results and prove the efficiency of the process. Furthermore, the time between the use of the fiber for testing and its treatment with the chemical process will be studied since can be a critical parameter for optical fiber reuse. Other methods of treatment are intended to apply to compare results between processes.

To be able to evaluate the sensor surface in more detail both in terms of functionalization and after chemical treatment for reuse, besides SEM and ATR-FTIR it is planned to characterize the biosensors by atomic force microscopy (AFM) since it is a scanning microscopy technique with very high resolution in the order of fractions of nanometer.

References

[1] V. Pinto, P. Sousa, S. O. Catarino, M. Correia-Neves, and G. Minas, "Microfluidic immunosensor for rapid and highly-sensitive salivary cortisol quantification," *Biosens. Bioelectron.*, vol. 90, no. November 2016, pp. 308–313, 2017.

[2] A. Kaushik, A. Vasudev, S. K. Arya, S. K. Pasha, and S. Bhansali, "Recent advances in cortisol sensing technologies for point-of-care application," *Biosens. Bioelectron.*, vol. 53, pp. 499–512, 2014.

[3] S. P. Usha, A. M. Shrivastav, and B. D. Gupta, "A contemporary approach for design and characterization of fiber-optic-cortisol sensor tailoring LMR and ZnO/PPY molecularly imprinted film," *Biosens. Bioelectron.*, vol. 87, pp. 178–186, 2017.

[4] E. Commission, "Sustainable Development." [Online]. Available: https://ec.europa.eu/environment/eussd/. [Accessed: 01-Feb-2021].

[5] K. Ogawa, F. Ito, M. Nagae, T. Nishimura, M. Yamaguchi, and A. Ishimatsu, "Effects of Acid Stress on Reproductive Functions in Immature Carp, Cyprinus Carpio," *Water, Air, Soil Pollut.*, vol. 130, pp. 887–892, 2001.

[6] A. P. F. Turner, I. Karube, and G. S. Wilson, *Biosensors: fundamentals and applications*, vol. 201. Oxford University Press, 1987.

[7] C. Leitão *et al.*, "Cortisol AuPd plasmonic unclad POF biosensor," *Biotechnol. Reports*, vol. 29, pp. 1–6, 2021.

[8] C. Leitao *et al.*, "Cortisol In-Fiber Ultrasensitive Plasmonic Immunosensing," *IEEE Sens. J.*, vol. 21, pp. 3028–3034, 2021.

[9] M. Zea *et al.*, "Electrochemical sensors for cortisol detections: Almost there," *Trends Anal. Chem.*, vol. 132, pp. 1–11, 2020.

[10] S. Shukla, N. K. Sharma, and V. Sajal, "Sensitivity enhancement of a surface plasmon resonance based fiber optic sensor using ZnO thin film: A theoretical study," *Sensors Actuators, B Chem.*, vol. 206, pp. 463–470, 2015.

[11] M. S. Soares *et al.*, "Immunosensing Based on Optical Fiber Technology: Recent Advances," *Biosensors*, vol. 11, no. 9: 305, pp. 1–35, 2021.

[12] A. Patnaik, K. Senthilnathan, and R. Jha, "Graphene-Based Conducting Metal Oxide Coated D-Shaped Optical Fiber SPR Sensor," *IEEE Photonics Technol. Lett.*, vol. 27, no. 23, pp. 2437–2440, 2015.

[13] H. Selye, "A syndrome produced by diverse nocuous agents," 1936.

[14] H. Selye, "The evolution of the stress concept," *Am Sci*, vol. 61, no. 6, pp. 692–699, 1973.

[15] F. Holsboer and M. Ising, "Stress Hormone Regulation: Biological Role and Translation into Therapy," *Annu. Rev. Psychol.*, vol. 61, no. 1, pp. 81–109, 2010.

[16] S. Dalirirad and A. J. Steckl, "Aptamer-based lateral flow assay for point of care cortisol detection in sweat," *Sensors Actuators, B Chem.*, vol. 283, no. November 2018, pp. 79–86, 2019.

[17] K. P. Wright *et al.*, "Influence of sleep deprivation and circadian misalignment on cortisol, inflammatory markers, and cytokine balance," *Brain. Behav. Immun.*, vol. 47, no. January, pp. 24–34, 2015.

[18] E. Russell, G. Koren, M. Rieder, and S. H. M. Van Uum, "The detection of cortisol in human sweat: Implications for measurement of cortisol in hair," *Ther. Drug Monit.*, vol. 36, pp. 30–34, 2014.

[19] N. Laboratories, *Male Blood Profile*, vol. 44, no. 0. 2018, pp. 1–2.

[20] P. M. Kabra, L. L. Tsai, and L. J. Marton, “Improved liquid-chromatographic method for determination of serum cortisol,” *Clin. Chem.*, vol. 25, no. 7, pp. 1293–1296, 1979.

[21] G. E. Abraham, J. E. Buster, and R. C. Teller, “Radioimmunoassay of plasma cortisol,” *Anal. Lett.*, vol. 5, no. 11, pp. 757–765, 1972.

[22] H. J. Ruder, R. L. Guy, and M. B. Lipsett, “A Radioimmunoassay for Cortisol in Plasma and Urine,” *J. Clin. Endocrinol. Metab.*, vol. 35, no. 2, pp. 219–224, 1972.

[23] Y. Kobayashi, K. Amitani, F. Watanabe, and K. Miyai, “Fluorescence polarization immunoassay for cortisol,” *Clin. Chim. Acta*, vol. 92, no. 2, pp. 241–247, 1979.

[24] D. Appel, R. D. Schmid, C. A. Dragan, M. Bureik, and V. B. Urlacher, “A fluorimetric assay for cortisol,” *Anal. Bioanal. Chem.*, vol. 383, no. 2, pp. 182–186, 2005.

[25] J. G. Lewis and P. A. Elder, “An enzyme-linked immunosorbent assay (ELISA) for plasma cortisol,” *J. Steroid Biochem.*, vol. 22, no. 5, pp. 673–676, 1985.

[26] M. Shimada, K. Takahashi, T. Ohkawa, M. Segawa, and M. Higurashi, “Determination of Salivary Cortisol by ELISA and Its Application to the Assessment of the Circadian Rhythm in Children,” *Horm. Res. Paediatr.*, vol. 44, pp. 213–217, 1995.

[27] B. Sadoul and B. Geffroy, “Measuring cortisol, the major stress hormone in fishes,” *J. Fish Biol.*, vol. 94, no. 4, pp. 540–555, 2019.

[28] E. Fanouraki, N. Papandroulakis, T. Ellis, C. C. Mylonas, A. P. Scott, and M. Pavlidis, “Water cortisol is a reliable indicator of stress in European sea bass, Dicentrarchus labrax,” *Behaviour*, vol. 145, no. 10, pp. 1267–1281, 2008.

[29] V. C. Mota, C. I. M. Martins, E. H. Edinga, A. V. M. Canário, and J. A. J. Verretha, “Steroids accumulate in the rearing water of commercial recirculating aquaculture systems,” *Aquac. Eng.*, vol. 62, no. 1, pp. 9–16, 2014.

[30] M. A. Najeeb, Z. Ahmad, R. A. Shakoor, A. M. A. Mohamed, and R. Kahraman, “A novel classification of prostate specific antigen (PSA) biosensors based on transducing elements,” *Talanta*, vol. 168, no. February, pp. 52–61, 2017.

[31] H. H. Nguyen, S. H. Lee, U. J. Lee, C. D. Fermin, and M. Kim, “Immobilized Enzymes in Biosensor Applications,” *Materials (Basel).*, vol. 12, no. 1, pp. 1–34, 2019.

[32] P. Mehrotra, “Biosensors and their applications - A review,” *J. Oral Biol. Craniofacial Res.*, vol. 6, no. 2, pp. 153–159, 2016.

[33] P. Damborský, J. Švitel, and J. Katrlík, “Optical biosensors,” *Essays Biochem.*, vol. 60, no. 1, pp. 91–100, 2016.

[34] M. D. Marazuela and M. C. Moreno-bondi, “Fiber-optic biosensors – an overview,” pp. 664–682, 2002.

[35] R. C. Stevens, S. D. Soelberg, S. Near, and C. E. Furlong, “Detection of cortisol in saliva with a flow-filtered, portable surface plasmon resonance biosensor system,” *Anal. Chem.*, vol. 80, no. 17, pp. 6747–6751, 2008.

[36] S. Jo *et al.*, “Localized surface plasmon resonance aptasensor for the highly sensitive direct detection of cortisol in human saliva,” *Sensors Actuators, B Chem.*, vol. 304, no. August 2019, p. 127424, 2020.

[37] K. Sun, N. Ramgir, and S. Bhansali, “An immunoelectrochemical sensor for salivary cortisol measurement,” *Sensors Actuators, B Chem.*, vol. 133, no. 2, pp. 533–537, 2008.

[38] Y. H. Kim *et al.*, “Direct immune-detection of cortisol by chemiresistor graphene oxide sensor,” *Biosens. Bioelectron.*, vol. 98, no. June, pp. 473–477, 2017.

[39] K. S. Kim *et al.*, “Highly sensitive and selective electrochemical cortisol sensor using bifunctional protein interlayer-modified graphene electrodes,” *Sensors Actuators, B Chem.*, vol. 242, pp. 1121–1128, 2017.

[40] C. Cristea, A. Florea, M. Tertiș, and R. Săndulescu, “Immunosensors,” in *Biosensors - Micro and Nanoscale Applications*, T. Rinken, Ed. IntechOpen, 2015, pp. 165–202.

[41] M. Alzawa, “Immunosensors for clinical analysis,” vol. 31, 1994.

[42] W. Gong *et al.*, “Experimental and theoretical investigation for surface plasmon resonance biosensor based on graphene/Au film/D-POF,” *Opt. Express*, vol. 27, no. 3, p. 3483, 2019.

[43] H. Kadhum Hisham, “Optical Fiber Sensing Technology: Basics, Classifications and Applications,” *Am. J. Remote Sens.*, vol. 6, pp. 1–5, 2018.

[44] B. Culshaw and A. Kersey, “Fiber-Optic Sensing : A Historical Perspective,” *J. Light. Technol.*, vol. 26, no. 9, pp. 1064–1078, 2008.

[45] V. Giurgiutiu, “Fiber-Optic Sensors,” in *Structural Health Monitoring of Aerospace Composites*, V. Giurgiutiu, Ed. Academic Press, 2016, pp. 249–296.

[46] R. N. Lopes, D. M. C. Rodrigues, R. C. S. B. Allil, and M. M. Werneck, “Plastic optical fiber immunosensor for fast detection of sulfate-reducing bacteria,” *Measurement*, vol. 125, no. September 2017, pp. 377–385, 2018.

[47] S. Sridevi, K. S. Vasu, S. Sampath, S. Asokan, and A. K. Sood, “Optical detection of glucose and glycated hemoglobin using etched fiber Bragg gratings coated with functionalized reduced graphene oxide,” *J. Biophotonics*, vol. 9, no. 7, pp. 760–769, 2016.

[48] N. Cennamo *et al.*, “Detection of naphthalene in sea-water by a label-free plasmonic optical fiber biosensor,” *Talanta*, vol. 194, pp. 289–297, 2019.

[49] G. P. Anderson and C. R. Taitt, *Evanescent wave fiber optic biosensors*, Second Edi. Elsevier B.V., 2008.

[50] M. jie Yin, B. Gu, Q. F. An, C. Yang, Y. L. Guan, and K. T. Yong, “Recent development of fiber-optic chemical sensors and biosensors: Mechanisms, materials, micro/nano-fabrications and applications,” *Coord. Chem. Rev.*, vol. 376, pp. 348–392, 2018.

[51] B. Liedberg, C. Nylander, and I. Lunström, “Surface plasmon resonance for gas detection and biosensing,” *Sensors and Actuators*, vol. 4, pp. 299–304, 1983.

[52] M. S. Aruna Gandhi, S. Chu, K. Senthilnathan, P. R. Babu, K. Nakkeeran, and Q. Li, “Recent advances in plasmonic sensor-based fiber optic probes for biological applications,” *Appl. Sci.*, vol. 9, pp. 1–22, 2019.

[53] N. F. Chiu, C. Du Yang, C. C. Chen, T. L. Lin, and C. T. Kuo, *Functionalization of Graphene and Graphene Oxide for Plasmonic and Biosensing Applications*. Elsevier Inc., 2018.

[54] Y. Tang, X. Zeng, and J. Liang, “Surface plasmon resonance: An introduction to a surface spectroscopy technique,” *J. Chem. Educ.*, vol. 87, no. 7, pp. 742–746, 2010.

[55] X. Zhu and T. Gao, *Spectrometry*. Elsevier Inc., 2018.

[56] S. H. Kim and K. Koh, “Functional dyes for surface plasmon resonance-based sensing system,” in *Functional Dyes*, S.-H. Kim, Ed. Elsevier B.V., 2006, pp. 185–213.

[57] A. Otto, “Excitation of nonradiative surface plasma waves in silver by the method of frustrated total reflection,” *Zeitschrift für Phys.*, vol. 216, no. 4, pp. 398–410, 1968.

[58] Y. Zhao, R. jie Tong, F. Xia, and Y. Peng, “Current status of optical fiber biosensor based on surface plasmon resonance,” *Biosens. Bioelectron.*, vol. 142, pp. 1–12, 2019.

[59] J. Sun *et al.*, “Sensitive and selective surface plasmon resonance sensor employing a gold-supported graphene composite film/D-shaped fiber for dopamine detection,” *J. Phys. D. Appl. Phys.*, vol. 51, no. 19, 2019.

[60] T. Guo, Á. González-Vila, M. Loyez, and C. Caucheteur, “Plasmonic Optical Fiber-Grating Immunosensing: A review,” *Sensors (Switzerland)*, vol. 17, pp. 1–20, 2017.

[61] M. Loyez, M. Lobry, E. M. Hassan, M. C. DeRosa, C. Caucheteur, and R. Wattiez, “HER2 breast cancer biomarker detection using a sandwich optical fiber assay,” *Talanta*, vol. 221, pp. 1–8, 2021.

[62] N. M. Y. Zhang *et al.*, “Hybrid Graphene/Gold Plasmonic Fiber-Optic Biosensor,” *Adv. Mater. Technol.*, vol. 2, pp. 1–6, 2017.

[63] M. D. Stoller, S. Park, Y. Zhu, J. An, and R. S. Ruoff, “Graphene-Based Ultracapacitors,” pp. 6–10, 2008.

[64] A. S. Mayorov *et al.*, “Micrometer-scale ballistic transport in encapsulated graphene at room temperature,” *Nano Lett.*, vol. 11, no. 6, pp. 2396–2399, 2011.

[65] A. A. Balandin, “Thermal properties of graphene and nanostructured carbon materials,” *Nat. Mater.*, vol. 10, no. 8, pp. 569–581, 2011.

[66] R. R. Nair *et al.*, “Fine Structure Constant Defines Visual Transparency of Graphene,” *Science (80-.).*, vol. 320, no. 5881, pp. 1308–1308, 2008.

[67] F. Wang *et al.*, “Laser-induced graphene: preparation, functionalization and applications,” *Mater. Technol.*, vol. 33, no. 5, pp. 340–356, 2018.

[68] C. Liu *et al.*, “Graphene oxide functionalized long period grating for ultrasensitive label-free immunosensing,” *Biosens. Bioelectron.*, vol. 94, pp. 200–206, 2017.

[69] S. Kaushik, U. K. Tiwari, A. Deep, and R. K. Sinha, “Two-dimensional transition metal dichalcogenides assisted biofunctionalized optical fiber SPR biosensor for efficient and rapid detection of bovine serum albumin,” *Sci. Rep.*, vol. 9, no. 1, pp. 1–11, 2019.

[70] H. M. Kim, J. H. Park, and S. K. Lee, “Fiber optic sensor based on ZnO nanowires decorated by Au nanoparticles for improved plasmonic biosensor,” *Sci. Rep.*, vol. 9, no. 1, pp. 1–9, 2019.

[71] C. Caucheteur, T. Guo, and J. Albert, “Review of plasmonic fiber optic biochemical sensors: improving the limit of detection,” *Anal. Bioanal. Chem.*, vol. 407, pp. 3883–3897, 2015.

[72] K. Gasior, T. Martynkien, G. Wojcik, P. Mergo, and W. Urbanczyk, “D-shape polymer optical fibres for surface plasmon resonance sensing,” *Opto-Electronics Rev.*, vol. 25, pp. 1–5, 2017.

[73] A. Leung, P. M. Shankar, and R. Mutharasan, “A review of fiber-optic biosensors,” *Sensors Actuators B Chem.*, vol. 125, pp. 688–703, 2007.

[74] K. O. Hill, Y. Fujii, D. C. Johnson, and B. S. Kawasaki, “Photosensitivity in optical fiber waveguides: Application to reflection filter fabrication,” *Appl. Phys. Lett.*, vol. 32, no. 10, pp. 647–649, 1978.

[75] G. Meltz, W. W. Morey, and W. H. Glenn, “Formation of Bragg gratings in optical fibers by a transverse holographic method,” *Opt. Lett.*, vol. 14, no. 15, p. 823, 1989.

[76] T. Geernaert *et al.*, “Point-by-point fiber Bragg grating inscription in free-standing step-index and photonic crystal fibers using near-IR femtosecond laser,” *Opt. Lett.*, vol. 35, no. 10, pp. 1647–1649, 2010.

[77] A. Theodosiou, A. Lacraz, A. Stassis, C. Koutsides, M. Komodromos, and K. Kalli, "Plane-by-Plane Femtosecond Laser Inscription Method for Single-Peak Bragg Gratings in Multimode CYTOP Polymer Optical Fiber," *J. Light. Technol.*, vol. 35, no. 24, pp. 5404–5410, 2017.

[78] A. Iadicicco, S. Campopiano, A. Cutolo, M. Giordano, and A. Cusano, "Thinned fiber Bragg gratings for sensing applications," *Proc. WFOPC2005 - 4th IEEE/LEOS Work. Fibres Opt. Passiv. Components*, vol. 2005, pp. 204–209, 2005.

[79] H. Kumazaki, Y. Yamada, H. Nakamura, S. Inaba, and K. Hane, "Tunable wavelength filter using a Bragg grating fiber thinned by plasma etching," *IEEE Photonics Technol. Lett.*, vol. 13, no. 11, pp. 1206–1208, 2001.

[80] X. Dong, H. Zhang, B. Liu, and Y. Miao, "Tilted fiber bragg gratings: Principle and sensing applications," *Photonic Sensors*, vol. 1, no. 1, pp. 6–30, 2011.

[81] F. Chiavaioli, F. Baldini, S. Tombelli, C. Trono, and A. Giannetti, "Biosensing with optical fiber gratings," *Nanophotonics*, vol. 6, pp. 663–679, 2017.

[82] J.-M. Renoirt, C. Zhang, M. Debliquy, M.-G. Olivier, P. Mégret, and C. Caucheteur, "High-refractive-index transparent coatings enhance the optical fiber cladding modes refractometric sensitivity," *Opt. Express*, vol. 21, no. 23, p. 29073, 2013.

[83] S. Li *et al.*, "A polarization-Independent Fiber-Optic SPR Sensor," *Sensors*, vol. 18, pp. 1–10, 2018.

[84] G. Laffont and P. Ferdinand, "Tilted short-period fibre-Bragg-grating- induced coupling to cladding modes for accurate refractometry," *Meas. Sci. Technol.*, vol. 12, pp. 765–770, 2001.

[85] Y. Y. Shevchenko and J. Albert, "Plasmon resonances in gold-coated tilted fiber Bragg gratings," *Opt. Lett.*, vol. 32, no. 3, pp. 211–213, 2007.

[86] S. W. James and R. P. Tatam, "Optical fibre long-period grating sensors: Characteristics and application," *Meas. Sci. Technol.*, vol. 14, no. 5, pp. 49–61, 2003.

[87] J. W. Fleming, "Dispersion in GeO2–SiO2 glasses," *Appl. Opt.*, vol. 23, pp. 4486–4493, 1984.

[88] V. Markova, B. Ilieva, and B. Naydenov, "Guiding Properties of the Polymer Optical Fibers," in *ICEST*, 2011, pp. 247–250.

[89] P. B. Johnson and R. W. Christy, "Optical Constant of the Nobel Metals," *Phys. Rev. B*, vol. 6, pp. 4370–4379, 1972.

[90] K. Okamoto, *Fundamentals of Optical Waveguides*, 2th Editio. Academic Press, 2006.

[91] N. Cennamo, D. Massarotti, L. Conte, and L. Zeni, "Low Cost Sensors Based on SPR in a Plastic Optical Fiber for Biosensor Implementation," *Sensors*, vol. 11, pp. 11752–11760, 2011.

[92] N. Cennamo, M. Pesavento, and L. Zeni, "A review on simple and highly sensitive plastic optical fiber probes for bio-chemical sensing," *Sensors Actuators, B Chem.*, vol. 331, pp. 1–9, 2021.

[93] M. Iga, A. Seki, and K. Watanabe, "Gold thickness dependence of SPR-based hetero-core structured optical fiber sensor," *Sensors Actuators, B Chem.*, vol. 106, pp. 363–368, 2005.

[94] F. George, "Norma da Direção-Geral da Saúde: Diagnóstico e Classificação da Diabetes Mellitus," 2011.

[95] F. Mach *et al.*, "2019 ESC/EAS Guidelines for the management of dyslipidaemias: Lipid modification to reduce cardiovascular risk," *Eur. Heart J.*, vol. 41, no. 1, pp. 111–188, 2020.

[96] M. D. A. Pereira-da-silva and F. A. Ferri, “Scanning Electron Microscopy,” in *Nanocharacterization Techniques*, Elsevier Inc., 2017, pp. 1–35.

[97] J. Goldstein *et al.*, *Scanning Electron Microscopy and X-Ray Microanalysis*, 4th Editio., vol. 10, no. 3. New York: Springer Nature, 1992.

[98] D. Titus, E. James Jebaseelan Samuel, and S. M. Roopan, “Nanoparticle characterization techniques,” in *Green Synthesis, Characterization and Applications of Nanoparticles*, A. K. Shukla and S. Iravani, Eds. Elsevier Inc., 2019, pp. 303–319.

[99] T. C. Lovejoy *et al.*, “Single atom identification by energy dispersive x-ray spectroscopy,” *Appl. Phys. Lett.*, vol. 100, no. 15, pp. 1–4, 2012.

[100] J. J. Feng, X. X. Lin, S. S. Chen, H. Huang, and A. J. Wang, “Thymine-directed synthesis of highly branched gold-palladium alloy nanobrambles as a highly active surface-enhanced Raman scattering substrate,” *Sensors Actuators, B Chem.*, vol. 247, pp. 490–497, 2017.

[101] J. Konopka, “Options for Quantitative Analysis of Light Elements by SEM/EDS,” *Thermo Fish. Sci.*, pp. 1–4, 2013.

[102] M. A. Mohamed, J. Jaafar, A. F. Ismail, M. H. D. Othman, and M. A. Rahman, “Fourier Transform Infrared (FTIR) Spectroscopy,” in *Fourier Transform Infrared (FTIR) Spectroscopy*, Elsevier B.V., 2017, pp. 3–29.

[103] A. Subramanian and L. Rodriguez-saona, “Fourier Transform Infrared (FTIR) Spectroscopy,” in *Infrared Spectroscopy for Food Quality Analysis and Control*, D.-W. Sun, Ed. Elsevier Inc., 2009, pp. 145–178.

[104] P. J. Larkin, “Instrumentation and Sampling Methods,” in *Infrared and Raman Spectroscopy*, Second Edi., Elsevier Inc., 2018, pp. 29–61.

[105] A. Shrivastava and V. B. Gupta, “Methods for the determination of limit of detection and limit of quantitation of the analytical methods,” *Chronicles Young Sci.*, vol. 2, p. 21, 2011.

[106] J. K. Dae, R. Pitchimani, D. E. Snow, and L. J. Hope-Weeks, “A Simple Method for the Removal of Thiols on Gold Surfaces Using an NH4OH-H2O2-H2O Solution,” *Scanning*, vol. 30, no. 2, pp. 118–122, 2008.